

All-Inorganic Cesium-Based Hybrid Perovskites for Efficient and Stable Solar Cells and Modules

Riccardo Montecucco, Eleonora Quadri, Riccardo Po, and Giulia Grancini*

In the last ten years, organic–inorganic hybrid perovskites have been skyrocketing the field of innovative photovoltaics (PVs) and now represent one of the most promising solution for next-generation PVs. Within the family of halide perovskites, increasing attention has been focused on the so-called all-inorganic group, where the organic cation is replaced by cesium, as in the case of CsPbI₃. This subclass of halide perovskites features desirable optoelectronic properties such as easily tunable bandgap, strong defect tolerance, and improved thermal stability compared to the hybrid systems. When integrated in PV cells, they exhibit high power conversion efficiency (PCE) with record values of 19.03%. However, all-inorganic perovskite solar cells (PSCs) face several challenges such as i) instability of the CsPbI₃ photoactive phase in ambient conditions, ii) inhomogeneous film morphology, and iii) high surface defect density. This work focuses on the mentioned challenges with a special attention on discussing the Cs–Pb–X system (X = I, Br). Then, the most recent and effective approaches for increasing both the PCE and the stability of devices are reviewed, which include material doping, interface engineering, and device optimization. Finally, the first efforts toward the upscaling of Cs-based PSCs, and predicted methods for enabling large-scale production, are discussed.

high defect tolerance, long carrier diffusion length, and compatibility toward scalable manufacturing processes to name a few.^[2–7] However, hybrid perovskites face severe degradation issues under operative conditions, which stem from the (photo) chemical instability when exposed to moisture, oxygen, UV light, and heat.^[8–12] Among other reasons, the presence of the hydrophobic organic cation, e.g., methylammonium, can accelerate the degradation path.^[12–14] For this reason, a greater focus has been devoted to exploring inorganic elements to replace the organic cations, for instance, using cesium to form CsPbX₃ all-inorganic perovskites. This system has been revealed of particular interest especially for the improved thermal stability of the material and, consequently, the enhanced device lifetime.^[13] CsPbI₃ and CsPbBr₃ are the most studied materials within this class, with a rapid boost of their use for highly efficient solar cells, reaching 19.03% in 2019.^[15]


However, the PCE of CsPbX₃-based devices are still lower than their organic–inorganic counterparts and far from the Shockley–Queisser limit calculated for their bandgap.^[16] Therefore, major efforts are required to stabilize the CsPbI₃ structure and to fabricate high quality CsPbX₃ thin films, before upscaling the manufacturing toward marketable devices. In this work, we provide a compelling perspective on the most recent and innovative strategies to tackle this challenge. The structural and optoelectronic properties of CsPbX₃ materials are first sorted out, with a focus on the film morphology, crystal structure, and phase transitions of each system. Second, methods for improving the photovoltaic performances and the stability of CsPbX₃-based devices are reported, focusing on the highest PCE and the longest device lifetimes reported up to date. Finally, we provide a perspective on the state of the art and future challenges for the upscaling of all-inorganic perovskite modules.

1. Introduction

During the last decade, hybrid halide perovskites solar cells have demonstrated power conversion efficiencies (PCEs) above 25%, approaching that of more mature technologies such as silicon (26.7%).^[1] They possess unique optoelectronic properties such as high absorption coefficient, bandgap tunability,

R. Montecucco, Prof. G. Grancini
Department of Chemistry and INSTM
University of Pavia
Via T. Taramelli 14, Pavia 27100, Italy
E-mail: giulia.grancini@unipv.it

E. Quadri, R. Po
Eni S.p.A.
Via Giacomo Fauser 4, Novara 28100, Italy

 The ORCID identification number(s) for the author(s) of this article can be found under <https://doi.org/10.1002/aenm.202100672>.

© 2021 The Authors. Advanced Energy Materials published by Wiley-VCH GmbH. This is an open access article under the terms of the Creative Commons Attribution-NonCommercial-NoDerivs License, which permits use and distribution in any medium, provided the original work is properly cited, the use is non-commercial and no modifications or adaptations are made.

DOI: 10.1002/aenm.202100672

2. All-Inorganic Perovskites Materials: Crystal Structure and Optoelectronic Properties

2.1. Cesium Lead Iodide Thin Films

So far, CsPbI₃ has been the most studied all-inorganic Cs-based halide perovskite for PVs, thanks to its bandgap of 1.7 eV (suitable for solar spectrum absorption) and long charge carrier

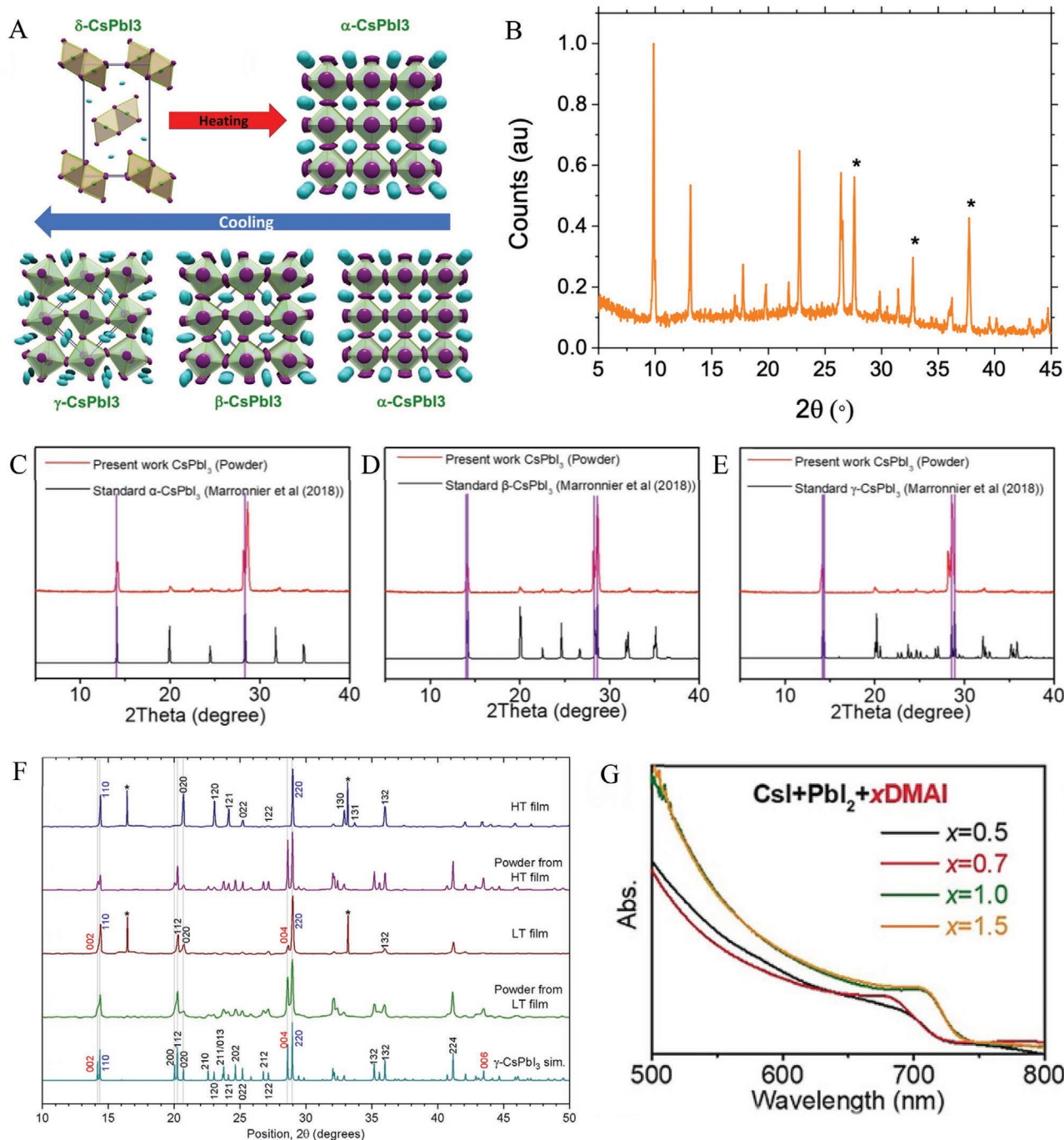


Figure 1. A) The four different structural phases of CsPbI_3 and the phase transition involved. Reproduced with permission.^[18] Copyright 2018, American Chemical Society. B) X-ray diffraction pattern of CsPbI_3 δ yellow phase. Peaks marked with an * are assigned to the FTO substrate. Reproduced with permission.^[19] Copyright 2015, Royal Society of Chemistry. C–E) XRD pattern comparison between CsPbI_3 powder from ref. ^[21] and standard α , β , γ - CsPbI_3 , respectively. Reproduced with permission.^[21] Copyright 2019, American Association for the Advancement of Science. F) XRD pattern comparison between thin films prepared with different methods, powder scratched from them, and simulated pattern for γ - CsPbI_3 . Adapted with permission.^[20] Copyright 2018, American Chemical Society. G) Absorption spectra of CsPbI_3 prepared with different concentrations of DMAI. The two different absorption onsets stem from two different phases. Adapted with permission.^[15] Copyright 2019, Wiley.

mobility.^[17] From a structural point of view, all-inorganic Cs-based halide perovskites can form into four different crystal phases: cubic (α), tetragonal (β), and two orthorhombic phases (called a black γ phase and a nonperovskite yellow δ phase) (see image in **Figure 1A**).^[18] The thermodynamically stable phase at

room temperature of the CsPbI_3 is the yellow δ phase. It is characterized by a main diffraction peak at around 10° (Figure 1B) and has a wide bandgap of 2.95 eV.^[19] By annealing the material above 310°C , a phase transition occurs to the black cubic perovskite phase, showing its strongest peaks at around 15°

and 29° (Figure 1C).^[19,20] On the other hand, by slowly cooling down the sample, Marronnier et al. reported that the α -CsPbI₃ structure converts at 260 °C to the tetragonal β -phase and at 175 °C to the γ -phase, both of which are black (X-ray diffraction (XRD) patterns are reported in Figure 1D,E).^[18] Evidence for the γ -phase comes from the presence of a peak splitting of the three characteristic perovskite peaks near 15°, 20°, and 30° angle, suggestive of an orthorhombic structure (Figure 1E).^[20] Only after a few days, especially if the sample is exposed to moisture and air, the yellow δ -phase may appear again. Noticeably, these phase transitions do not occur in the reversed direction when the δ -phase is heated, forming directly the α -phase.^[20]

For application in optoelectronic devices, it is important to determine which polymorph is adopted by thin films of CsPbI₃. By comparing the XRD pattern of thin films prepared with different synthetic routes and powders scratched from them, Sutton et al. have prepared films with black γ -phase at room temperature via high temperature (HT) annealing and low-temperature (LT) additive incorporation (Figure 1F).^[20] In both cases, the XRD patterns show a preferred orientation, not present in the powder patterns. More in details, i) the HT film exhibits a strong peaks at $[hk0]$ directions while peaks from the $[00l]$ family were absent; ii) in contrast, the latter were present in the LT additive-mediated films, indicating in both cases a marked preferential crystal orientation, despite in a different direction.^[20] Another work has proven that most of the previously reported CsPbI₃ thin film XRD patterns have been incorrectly indexed to the α -phase and they correspond to the γ or β -phase.^[21] To determine that, absorption spectra comparison allows for their identification. As shown in Figure 1G, it is evident that γ -phase CsPbI₃ ($x = 0.5, 0.7$) has a direct bandgap at 1.73 eV, which corresponds to an absorption onset of about 717 nm, while the β -phase ($x = 1.0, 1.5$) has an absorption onset at about 736 nm (bandgap of 1.68 eV).^[15] This descending trend has also been rationalized in terms of degree of distortion away from the cubic structure through first principle calculations.^[15,18,21]

2.2. Cesium Lead Bromide Thin Films

CsPbBr₃ has been among the first cesium-based lead halide perovskite investigated because of its outstanding stability under ambient conditions.^[22] That is due to the increased Goldsmith tolerance factor as a consequence of the smaller atomic radius of bromine compared to iodine.^[23] Similar to its iodine counterpart, CsPbBr₃ possesses a crystal structure made up by a 3D framework of corner sharing [PbBr₆]⁴⁻ octahedra, with Cs⁺ ions incorporated between the octahedral spaces. CsPbBr₃ crystallizes in a yellow orthorhombic phase (*Pnma*) at room temperatures and upon heating it undergoes phase transition to yellow tetragonal (*P4/mbm*) and yellow-orange cubic (*Pm-3m*) phases at 88 and 130 °C, respectively.^[24] The typical XRD pattern of CsPbBr₃ displays peaks at about 15.20°, 21.55°, 26.48°, 30.66°, 34.37°, and 37.77° (depending on preparation method), which can be assigned to (100), (110), (111), (200), (210) and^[30–33] (211) lattice planes.^[25–27] Compared to CsPbI₃, CsPbBr₃ has a wider direct bandgap of ≈ 2.3 eV, which corresponds to an absorption onset around 540 nm (Figure 2A).^[28]

In addition to the CsPbBr₃ phase, the Cs–Pb–Br system allows two other derivative phases, CsPb₂Br₅ and Cs₄PbBr₆, with a bandgap of about 3.2 and 3.8, respectively (Figure 2A), which can coexist with CsPbBr₃ in thin films due to similar formation enthalpies.^[29] CsPb₂Br₅ shows a tetragonal 2D layer structure, where the Cs⁺ ions lay between two layers of Pb–Br edge-sharing polyhedrons (Figure 2B). The formation of this phase is promoted by excess PbBr₂ according to Equations (1) and (2)



By annealing the tetragonal CsPb₂Br₅ phase over 300 °C, it is possible to reverse its formation and recover the CsPbBr₃ phase. In contrast, trigonal Cs₄PbBr₆ features a 0D structure with [PbBr₆]⁴⁻ octahedra separated by CsBr bridges (Figure 2B). In a similar fashion than CsPb₂Br₅, Cs₄PbBr₆ is formed in CsBr-rich conditions according to Equations (3) and (4)^[24,25]



Interestingly, the phase transition mechanism for the Cs–Pb–Br system in humid environment has been observed through in situ synchrotron XRD experiment.^[30] According to this study, H₂O molecules can permeate the Cs₄PbBr₆ structure and strip the CsBr component out from the crystal, inducing the phase transition toward CsPbBr₃. Similarly, water can interact with CsPbBr₃, changing the lead coordination number and promoting the transition toward the CsPb₂Br₅ phase (Figure 2C).^[30]

Several works in literature focus on the optimization of the development of a specific phase of the Cs–Pb–Br system: at one side, it has been demonstrated that by modifying the PbBr₂:CsBr ratio in different solvents (DMSO, H₂O) through dichloromethane-assisted antisolvent method, it is possible to obtain a unique phase with high purity (Figure 2D,E),^[30] while on the other side, pure CsPbBr₃ by a two-step deposition method using 2-methoxyethanol as CsBr solvent has been demonstrated.^[31] These results suggest the possibility to fine tune the phase composition of the material to achieve surface passivation and PV performance improvements.

2.3. All-Inorganic Mixed Halide Perovskites Thin Films

To combine the enhanced stability at room temperature of the Br-compound with the extended absorption profile of the iodine one (essential to push the PCE), mixed compounds in the form of CsPb(I_{*x*}Br_{1–*x*})₃ have attracted a lot of interest since 2016.^[28] In the mixed halide compound CsPbI₂Br, compared to CsPbI₃, the orthorhombic-to-cubic transition temperature is reduced, happening at 250° instead of 350°, which is ascribed to an increased tolerance factor, responsible for better structural stability (see the disappearance of the peak at 10° characteristic of the delta phase; Figure 3A,B).^[32] These materials also present increased stability toward photoinduced phase segregation, which can seriously damage the device.^[33,34]

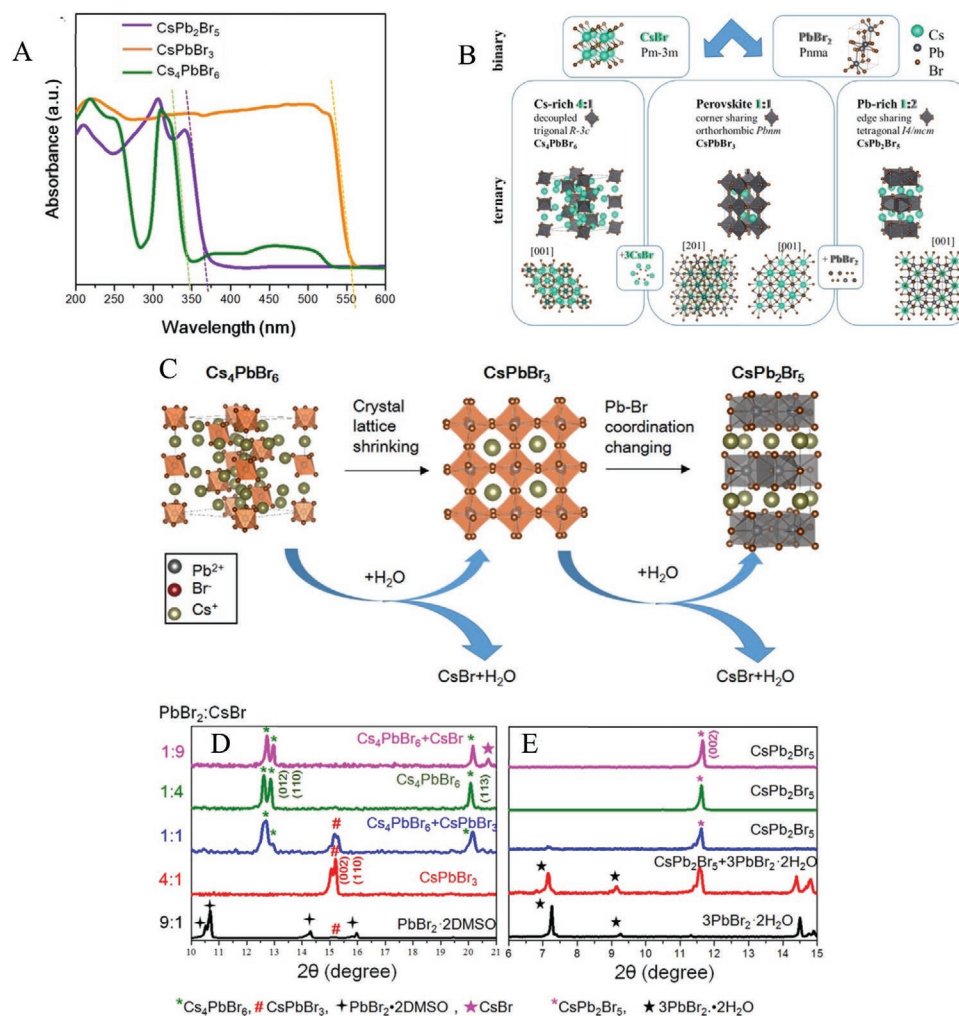


Figure 2. A) UV-vis absorption spectra of CsPbBr₃ and the derivative phases Cs₄PbBr₆ and CsPb₂Br₅. Reproduced with permission.^[30] Copyright 2018, American Chemical Society. B) Crystal structure of CsBr, PbBr₂, CsPbBr₃, and the derivative phases Cs₄PbBr₆ and CsPb₂Br₅. Adapted with permission.^[29] Copyright 2019, American Chemical Society. C) Scheme of the possible phase transition mechanism for Cs₄PbBr₆ into CsPbBr₃ and CsPb₂Br₅. Adapted with permission.^[30] Copyright 2018, American Chemical Society. D) XRD patterns of thin films prepared with different precursors ratio in DMSO. Adapted with permission.^[30] Copyright 2018, American Chemical Society. E) XRD patterns of thin films prepared with different precursors ratio in water. Adapted with permission.^[30] Copyright 2018, American Chemical Society.

As a consequence of bromine doping into the crystal structure, the structural and optical properties of CsPb(I_xBr_{1-x})₃ materials vary as function of Br molar content. Since the atomic radius of Br is lower compared to the iodine, a shift toward higher angles of the XRD peaks can be noted as Br content increases (Figure 3C). At the same time, a blueshift of both the absorption onset and the photoluminescence peak, which increases with the Br content (Figure 3D,E).^[32,35] Therefore, the bandgap of the CsPb(I_xBr_{1-x})₃ can be tuned by adjusting the composition from 1.73 eV for pure CsPbI₃ to 2.3 eV for pure CsPbBr₃ (see images in Figure 3F).

2.4. Energetics and Defects

Determining the electronic band structure and defect properties of all-inorganic cesium lead halide perovskites is crucial to

further understand the electronic properties of the materials. Figure 4A–C shows the computed electronic structure for α , β , and γ -CsPbI₃,^[18] showing that all the three phases have a direct bandgap, which widens with increasing distortion from the cubic symmetry. The distortion is represented by the tilting of the [PbI₆]⁴⁻ octahedra, which induces a stabilization of the top valence band and destabilizes the bottom of the conduction band. As a consequence, the bandgap increases.^[18] To prove the electronic picture, similar calculations on the band structure of CsPbBr₃ and its derivative phase CsPb₂Br₅ have also been reported in Figure 4D,F.^[37]

On the other side, discrete attention has been focused on the energetics of intrinsic point defects in all-inorganic perovskites. For instance, first principle calculations have been used to investigate point defects in CsPbBr₃, determining their formation energy, concentration under different growth condition, and their energetic position inside the bandgap.^[38]

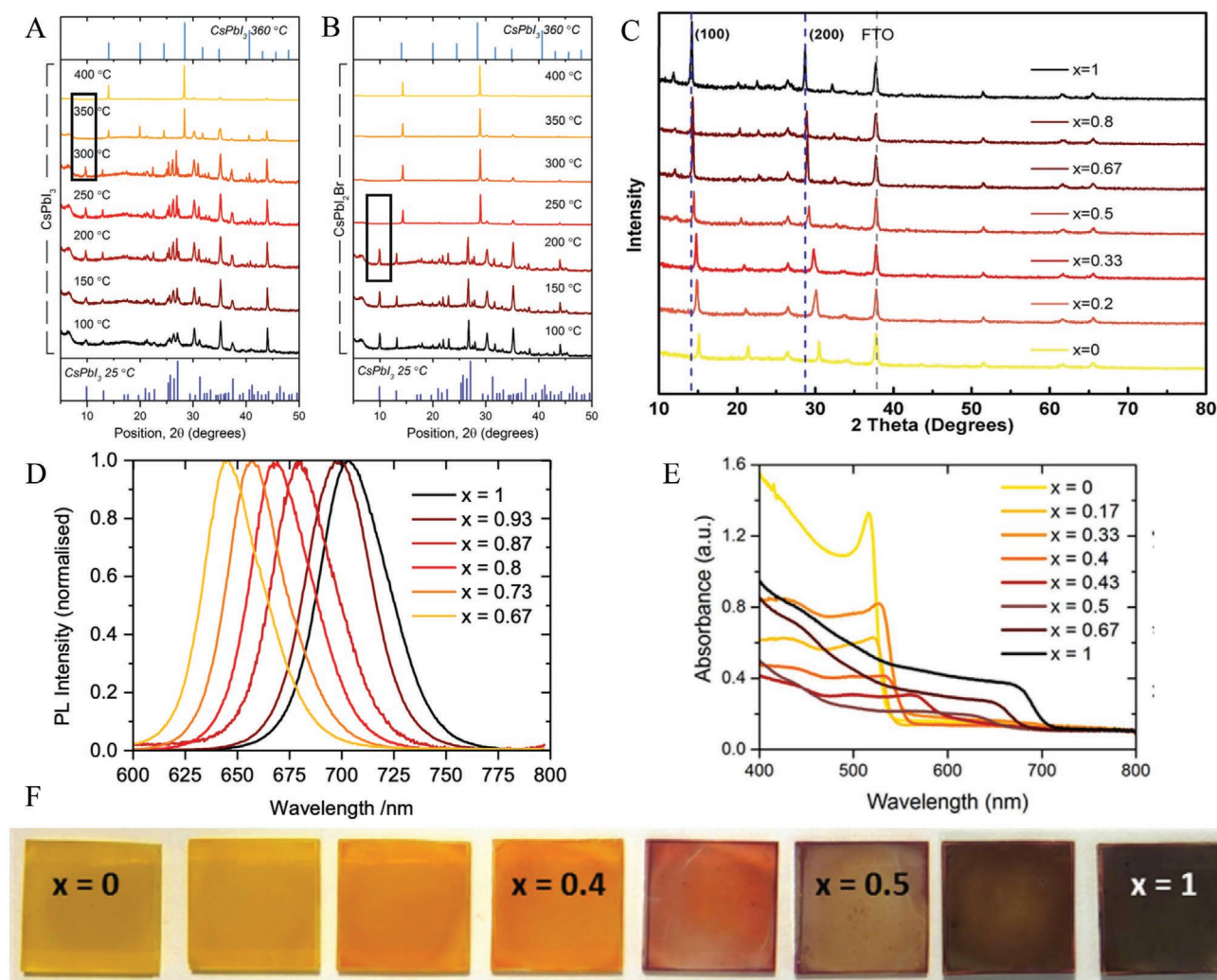


Figure 3. A) “In situ annealing” XRD diffraction pattern for CsPbI₃. The phase transition temperature is around 350 °C. Adapted with permission.^[32] Copyright 2016, Wiley. B) “In situ annealing” XRD diffraction pattern for CsPbBr₃. The phase transition temperature is around 250 °C. Adapted with permission.^[32] Copyright 2016, Wiley. C) XRD patterns of CsPb(I_xBr_{1-x})₃ thin films. Reproduced with permission.^[36] Copyright 2018, Elsevier. D) Steady-state photoluminescence spectra of CsPb(I_xBr_{1-x}) thin films. Reproduced with permission.^[32] Copyright 2016, Wiley. E) UV-vis absorption spectra of CsPb(I_xBr_{1-x}) thin films. Reproduced with permission.^[32] Copyright 2016, Wiley. F) Photographic images of CsPb(I_xBr_{1-x}) thin films. Reproduced with permission.^[32] Copyright 2016, Wiley.

The results show that under Br-rich condition, the dominant defect is the Cs vacancy (V_{Cs}), while Pb vacancy (V_{Pb}), Br interstitial (Br_i), and Cs substitution (Br_{Cs}) are also present due to their low formation energies.^[38] On the contrary, in Br-poor condition, the Br-vacancies become the most favored defect.^[38] Furthermore, the position of these defects relative to the conduction band minimum (CBM) and valence band maximum (VBM) has also been calculated. As clearly pictured in Figure 4G, most of the defects are shallow ones, which do not intact the optoelectronic properties of the material, while only Pb substitution (Pb_{Br}), Br-substitution (Br_{Pb}) and Pb interstitial (Pb_i) can introduce deep trap states, detrimental for recombination.^[39,40] Since the formation energies of deep-state defects are among the highest in all growth conditions, CsPbBr₃ is mainly affected by harmless shallow defects.

3. All-Inorganic Perovskite Solar Cells

3.1. Paths toward High Efficiency

In the recent years, several research groups have directed their efforts to increase the PCE of the all-inorganic Cs-based perovskite solar cells based on iodine and mixed halide, focusing on small device area (0.1 cm²).^[17,41,42] Strategies include precursor engineering, surface passivation/engineering, 2D/3D interface engineering, and architecture engineering.^[15,19,21,43–49] It is worth mentioning that most of the highest-efficiency single junction Cs-based all-inorganic PSCs are realized with the n-i-p structure, while there are only a few works describing high-efficiency p-i-n all-inorganic PSCs.^[50,51] This is mainly due to concomitant challenges in material and interface optimization in p-i-n configuration,^[51,52] leading to lower open circuit

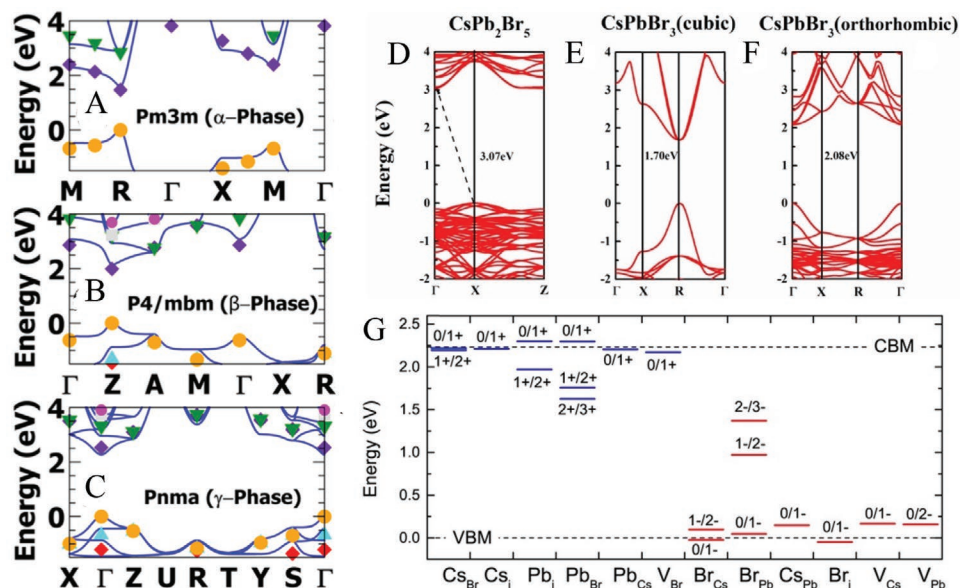


Figure 4. A–C) Calculated (lines) and experimental (symbols) band structure for the α , β , γ -CsPbI₃, respectively. Adapted with permission.^[18] Copyright 2018, American Chemical Society. D–F) Calculated band structure for CsPb₂Br₅, cubic CsPbBr₃, and orthorhombic CsPbBr₃, respectively. Adapted with permission.^[37] Copyright 2020, American Chemical Society. G) Defect charge transition levels calculated for CsPbBr₃. Reproduced with permission.^[38] Copyright 2017, American Chemical Society.

voltage,^[53] and poorer extracted current with respect to the n–i–p device. Despite recent advances, i.e., by Wang et al. optimizing the energy level alignment at the perovskite/electron transport layer interface by surface passivation achieving 16.1% PCE,^[53] and by Fu et al. demonstrating an effecting post-treatment agent to remove pinholes and passivate the CsPbI₃ film, achieving a record PCE of 16.67%,^[51] their efficiencies lag behind the records obtained with the n–i–p architecture of >19%. For this reason, we focus here on reviewing the methods and results developed so far for obtaining high efficiency single junction n–i–p devices, which can stimulate further advances that can be easily adopted on different solar cells architecture.^[15]

The first n–i–p device showing a remarkable efficiency has been reported by Eperon et al. in 2015. They introduced a low-temperature preparation method by mixing hydroiodic acid (HI) into the CsPbI₃ dimethylformamide (DMF) precursors solution.^[19] This method has revealed as a successful strategy to obtain a highly crystalline and stable black phase at around 100° due to the formation of dimethylammonium iodide (DMAI) as a consequence of the HI-catalyzed hydrolysis of the DMF.^[54] Further results suggested that the DMAI content can indeed significantly affect the crystal phase of the final CsPbI₃ perovskite by forming an intermediate perovskite phase, which turns into the desired CsPbI₃ phase during the annealing while releasing dimethylamine (Figure 5A).^[15] For this reason, follow up works have directly used DMAI to control the deposition of the film. For instance, Wang et al. have introduced DMAI into the CsPbI₃ precursor solution and, by properly tuning the stoichiometry, they obtained the black CsPbI₃ phase.^[21] Furthermore, the authors have developed a crack-filling interface engineering method through the deposition of choline iodide on top of the perovskite layer (Figure 5B), allowing for a better energy levels alignment and surface trap states passivation. Thanks to this approach, they have achieved in 2019 a state of the art

PCE of 18.4% and increased cell stability toward moisture and heat (see current–voltage (*J–V*) curve in Figure 5C).^[21] Interface engineering is indeed utmost to further push device efficiency. Indeed, the actual record PCE of 19.03% for all-inorganic Cs-based PSCs as to our best knowledge has been observed by passivating the perovskite/hole transport layer (HTL) interface with phenylethylammonium chloride (Figure 5D) and by optimizing the DMAI content in the precursors solution (see *J–V* curve in Figure 5E).^[15]

Combined with precursor engineering, surface passivation has proven to be a valuable method for improving the performances of the PSCs. For instance, a new strategy, which implies the incorporation of 4-aminobenzoic acid (ABA) into CsPbI₃ precursors solution and surface passivation with steric neostigmine bromide (NGBr), was proposed in 2020.^[43] In particular, the ABA molecules are absorbed at the surface of CsPbI₃ grains reducing the crystal distortion (they suppress the rotation of the PbI₆ octahedra by enhancing the energy barrier for the rotation) (Figure 6A). Furthermore, the NGBr passivation results in bromine enrichment and NG⁺ cation surface termination, which can further reduce the surface energy.^[43] Finally, both ABA molecules and NG⁺ cations can interact with shallow or deep-level defect thus reducing the defect density. The synergy between ABA and NGBr allowed to achieve a PCE of 18.27% (with n–i–p configuration) and enhanced stability (see *J–V* curves in Figure 6B).^[43] In fact, the NGBr–CsPbI₃(ABA) PSCs were able to retain up to 90% of their PCE after 500 h of white LED illumination and they showed no performance reduction after more than 200 h at 60% RH and 25 °C in N₂ glovebox.^[43]

As an alternative interface engineering approach, 2D perovskites on top of the 3D perovskite layer, commonly adopted for standard hybrid perovskites,^[55,56] have been recently used to reduce interfacial charge recombination and increase the all-inorganic perovskites resistance toward moisture. For instance,

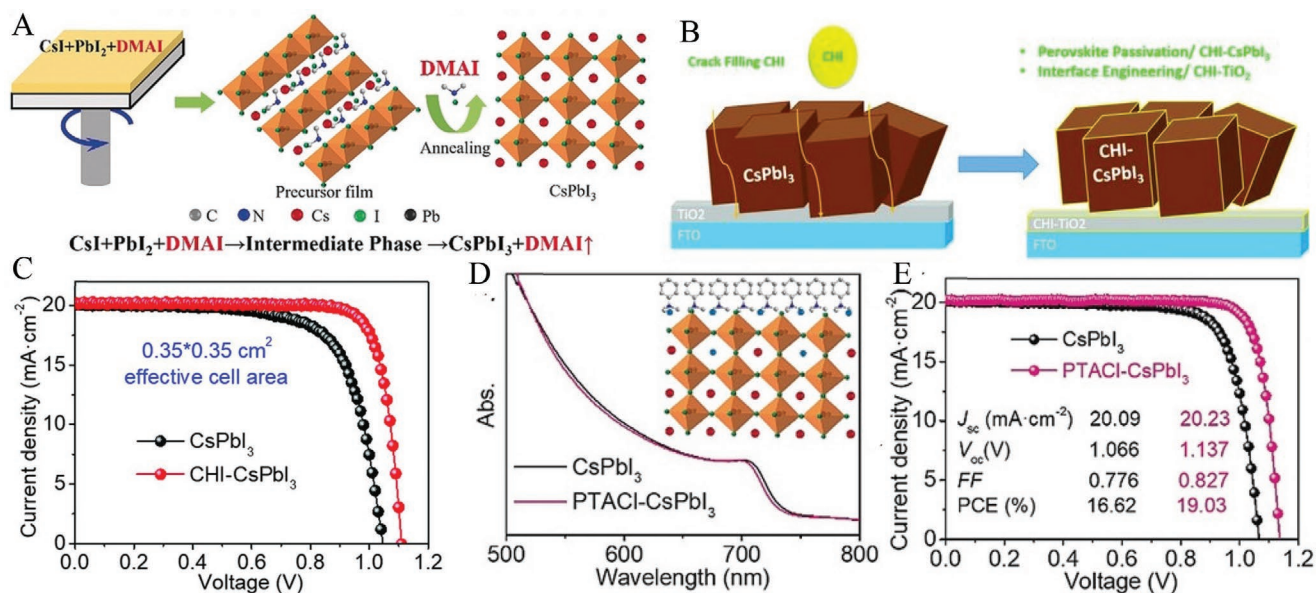


Figure 5. A) Schematic mechanism for DMAI additive induced black phase CsPbI₃ formation. Adapted with permission.^[15] Copyright 2019, Wiley. B) Schematic illustration of crack-filling engineering by choline iodide. Reproduced with permission.^[21] Copyright 2019, American Association for the Advancement of Science. C) *J*-*V* curve of PSCs based on CsPbI₃ and CHI-CsPbI₃ with 0.1 cm² effective cell area under simulated AM 1.5G solar illumination of 100 mW cm⁻² in reverse scan. Reproduced with permission.^[21] Copyright 2019, American Association for the Advancement of Science. D) UV/vis spectra of DMAI-based CsPbI₃ and PTACl-CsPbI₃ thin films. Reproduced with permission.^[15] Copyright 2019, Wiley. E) *J*-*V* curve of PSCs based on CsPbI₃ and PTACl-CsPbI₃ under simulated AM 1.5G solar illumination of 100 mW cm⁻² in reverse scan. Reproduced with permission.^[15] Copyright 2019, Wiley.

Yan et al. developed a guanidinium bromide (GABr) post-treatment process mainly consisting in the deposition of GABr on the CsPbI₃ film. As a result, the GA⁺ cation accumulates on the surface of the perovskite while a portion of the Br⁻ anion enters the perovskite lattice.^[48] This procedure also induced the formation of ultrathin GA-CsPbI_xBr_y perovskite on the surface of the CsPbI₃ grains. Together with the doped Br⁻ anions, the 2D perovskite can passivate surface defects and reduce the nonradiative recombination, thus improving the device performances. The authors report an enhanced PCE of 18.02% (*n-i-p* configuration) with optimized GABr concentration, mainly due to improved open circuit voltage (*V*_{oc}) and fill factor (FF).^[48] More recently, in 2020, the spontaneous self-assembly of a 2D/3D interface has been demonstrated, by adding guanidinium bromide (GABr) into the CsPbI₃ precursor solution. This phenomenon has been called spontaneous interfacial modification (SIM) (Figure 6C) because during the formation of CsPbI_xBr_{3-x} perovskite, GA cations are pushed up to the film surface and combine with the unsaturated Pb²⁺ to spontaneously organize the ultrathin lower-dimensional perovskite crystalline. Thanks to this 2D/3D architecture, the authors were able to achieve a PCE of 18.06% with *n-i-p* configuration, the 81% of which is retained after 1000 h of storage in ambient air (see *J*-*V* curves in Figure 6D).^[47]

Several groups also demonstrated that modifying the interface between the electron transport layer (ETL) and the perovskite can lead to reduced voltage losses and increased PCE. Recently, Chang et al. have realized an ambient blade-coating-based fabrication method for high-efficiency CsPbI₃ PSCs by adding Zn(C₆F₅)₂ into the perovskite precursors solution (Figure 6E). They achieved a champion PCE of 19.00% in

an *n-i-p* configuration, which is among the highest reported to the best of our knowledge (see *J*-*V* curves and cell architecture in Figure 6F,G).^[44] Their experimental results proved that Zn(C₆F₅)₂ is mainly located at the SnO₂/perovskite interface, where it is chemisorbed on both SnO₂ and CsPbI₃ surface. This leads to the formation of an energy gradient at the interface between the two layers, thus improving the band alignment and enhancing the *V*_{oc} and FF. Furthermore, it has been demonstrated that Zn(C₆F₅)₂ can also suppress the trap formation inside the perovskite film and increase the charge carrier lifetime. Finally, the unencapsulated devices showed a minimal 2% PCE loss after 700 h of storage in ambient conditions (20% RH, 25 °C).^[44]

3.2. Paths toward Improved Stability

The stability of both the material and the devices is currently one of the most current critical issues.^[8] Despite a consensus statement on the procedure for testing PSCs stability has been reported,^[57] still, the conditions specified for the tests are often too mild or arbitrary, and do not allow for a meaningful comparison of the results.^[8] Nevertheless, efforts have been made by research groups to improve both the storage and the operational stability of the devices. Several strategies, such as anion and B-site doping, surface passivation, architecture engineering, and crystal-growth engineering, have been applied to increase the resistance of the material toward moisture, heat, and light exposure.^[17,46,58-61]

Regarding the B site doping, in 2020, Yao et al. reported a doping strategy to improve both the efficiency and the stability of the CsPbI₃-based device by adding Mn²⁺ ions into the per-

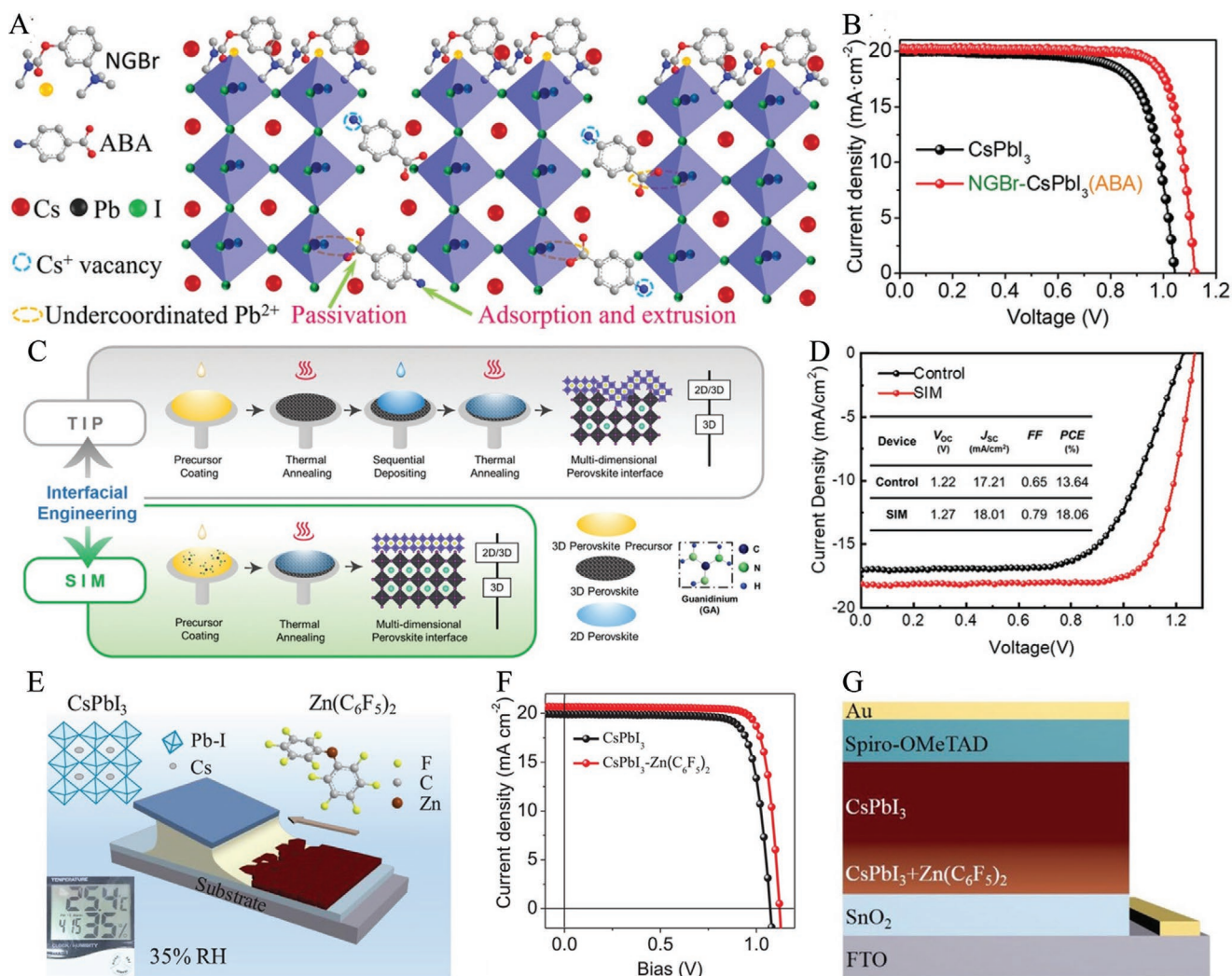


Figure 6. A) Schematic mechanism for the NGBr and ABA molecule interacted with CsPbI₃ inorganic perovskite. Reproduced with permission.^[43] Copyright 2020, Wiley. B) *J*-*V* curve of champion PSCs for the CsPbI₃ and NGBr-CsPbI₃(ABA)-based devices in reverse scan (effective cell area of 0.12 cm²). Reproduced with permission.^[43] Copyright 2020, Wiley. C) Schematic interfacial manipulation processing steps, where TIP and SIM stand for two-steps interfacial manipulation and spontaneous interfacial manipulation, respectively. Reproduced with permission.^[47] Copyright 2020, Wiley. D) *J*-*V* curve of the CsPbI₃Br_{3-x} PSCs with and without SIM. Reproduced with permission.^[47] Copyright 2020, Wiley. E) Schematic of blade-coating for the SnO₂, CsPbI₃ perovskite, and spiro-OMeTAD layers. The ambient humidity is ≈35% RH. Room temperature is ≈25 °C. The substrate temperature ranges from 25 to 100 °C. The Zn(C₆F₅)₂ is introduced into CsPbI₃ as an additive. Reproduced with permission.^[44] Copyright 2020, Wiley. F) *J*-*V* curves of the champion cell for the control CsPbI₃ and the CsPbI₃-Zn(C₆F₅)₂-based solar cells. Reproduced with permission.^[44] Copyright 2020, Wiley. G) Scheme showing a preferential accumulation of Zn(C₆F₅)₂ at the CsPbI₃/SnO₂ interface. Reproduced with permission.^[44] Copyright 2020, Wiley.

ovskite lattice.^[59] Since Mn²⁺ has the same octahedral coordination environment than Pb²⁺ while being smaller, its doping causes a contraction of the perovskite structure, which slows down the decomposition rate toward the photoinactive δ-phase thus improving the stability of the perovskite film.^[59] In fact, the Mn-doped film started to degrade after 8 days of aging test, while the pristine one showed degradation after only 2 days (Figure 7A). Furthermore, the PCE of the device was increased to 16.52% with 2% Mn²⁺ doping.^[59] As an alternative B site dopant, CaCl₂ has been introduced to the CsPbI₂Br precursors solution to enhance the crystal quality by lowering the perovskite crystallization rate, thus reducing the defect density and increasing the carrier lifetime of the CsPbI₂Br film, as well

as increase the Fermi level of the perovskite.^[58] The improved band alignment between the n-doped perovskite and the spiro HTL ultimately contributes to an increase in V_{OC} .^[58] Furthermore, by substituting the iodine with bromine and chlorine ions, it is possible to increase the value of the Goldsmith factor and consequently improving the stability of the perovskite cubic phase (Figure 7B).^[58] Thanks to this novel doping strategy, the authors have realized devices with a PCE of 16.79% (with n-i-p configuration), which is retained over 90% of its original value after more than 1000 h of storage in ambient air (Figure 7C).^[58]

As a different strategy, novel surface passivation method has been adopted by Chen et al. by depositing 18-crown-6 ether over the CsPbI₃ perovskite layer, in order to both suppress

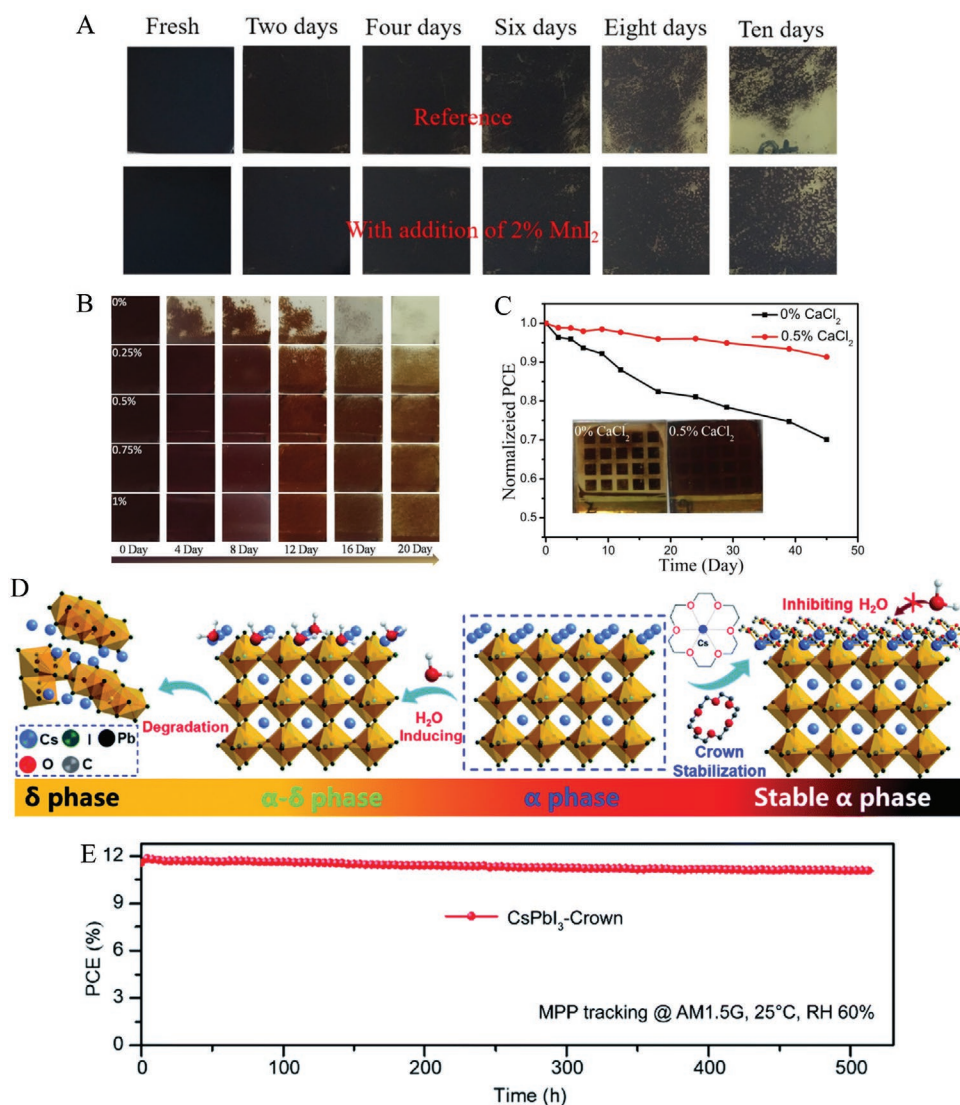


Figure 7. A) Photographs showing the thermal stability of the CsPbI₃ perovskite thin films without and with the addition of Mn at 80 °C in a glovebox filled with nitrogen. Reproduced with permission.^[59] Copyright 2020, Wiley. B) The photographs of CsPbI₂Br films with different concentrations of CaCl₂ additives aged in high humidity conditions (≈40%) for different durations. Reproduced with permission.^[58] Copyright 2020, Wiley. C) The air stability (humidity: ≈25%) of the control and optimized CsPbI₂Br PSCs. Reproduced with permission.^[58] Copyright 2020, Wiley. D) Schematic illustration of Crown passivating the surface of α -CsPbI₃, compared to the phase transformation from α -CsPbI₃ to δ -CsPbI₃. Inset is the chelation of Cs⁺ with Crown. Reproduced with permission.^[17] Copyright 2020, Royal Society of Chemistry. E) Operation stability of the encapsulated CsPbI₃-Crown PSC module under maximum power point tracking with air mass (AM) 1.5G irradiation at RH 60%. Reproduced with permission.^[17] Copyright 2020, Royal Society of Chemistry.

moisture penetration thanks to the aliphatic chain and passivate the defects through the coordination of Cs⁺ cations by the oxygen atoms (Figure 7D).^[17] This double role has allowed the successful blocking of the CsPbI₃ phase transition toward the δ -phase, thus achieving a PCE of 16.9% for the small area cells (0.1 cm²). More importantly, thanks to the strong coordination bond between Cs⁺ and oxygen atoms, the defect migration is suppressed, thus enhancing the stability of the devices. In fact, the latter retained more than 90% of their initial PCE after 2000 h of storage at 20% RH. Finally, the operational stability of encapsulated 8 cm² minimodules has also been studied by performing a maximum power point (MPP) tracking

experiment.^[17] Surprisingly, these modules retained 95.2% of their initial PCE after 500 h MPP tracking under 1 sun irradiation at 60% RH (Figure 7E).^[17]

To improve the bulk morphology, (adamantan-1-yl)methylammonium (ADMA) has been introduced as a soft-template controlled growth agent to produce pinhole-free CsPbI₃ perovskite films. By maximizing the nucleation rate at the initial stage of film formation and by carefully optimizing the annealing process, it was possible to regulate the growth rate through the gradual release of the ADMA cage (Figure 8A).^[62] The ADMA-CsPbI₃ n-i-p devices showed improved thermal stability when tested in N₂ at 60 °C compared to pristine-CsPbI₃

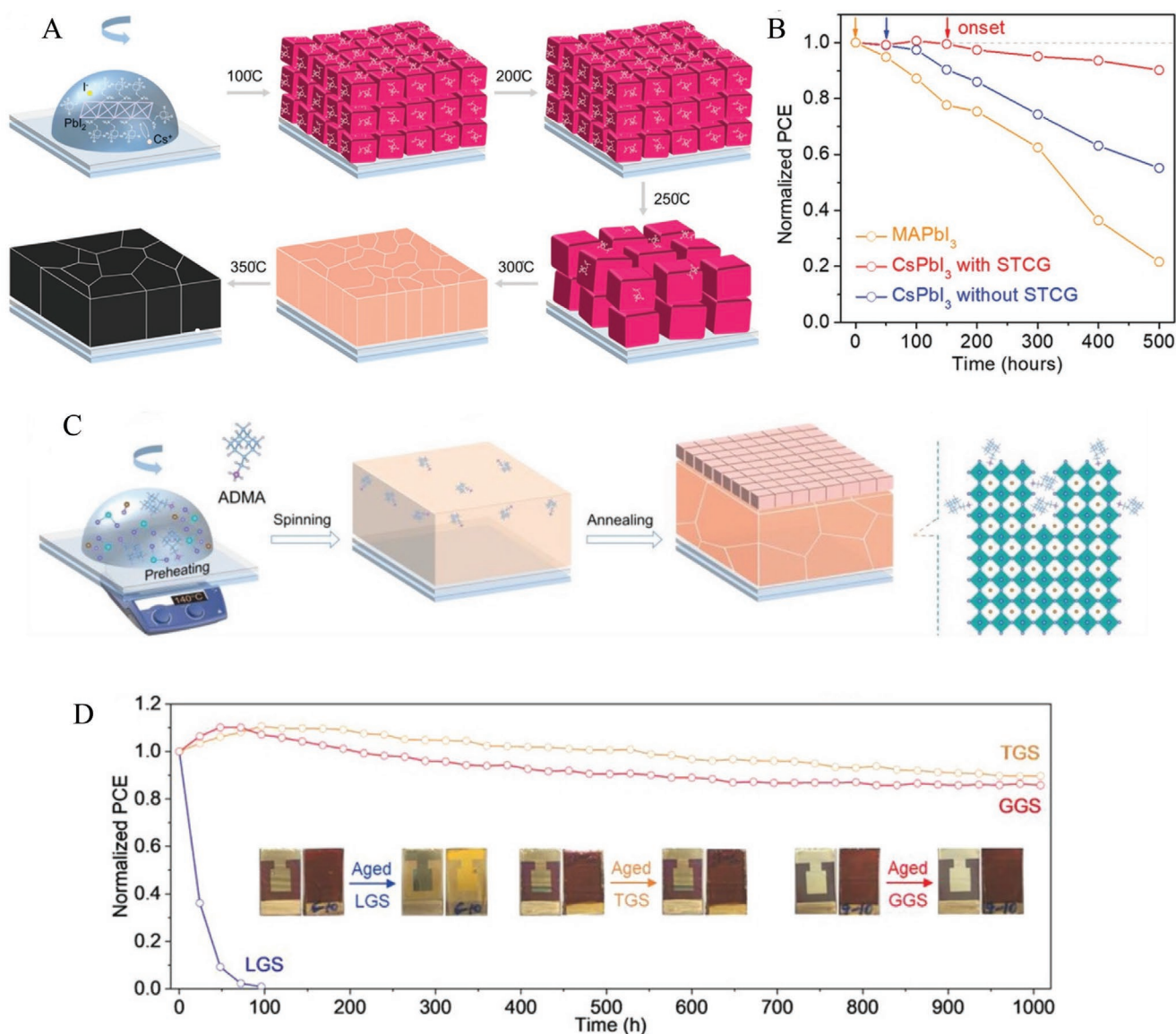


Figure 8. A) Processing scheme for a perovskite thin film using the soft-template controlled growth (STCG) method for the growth of CsPbI₃ film. Adapted with permission.^[62] Copyright 2020, Wiley. B) The long-term thermal stability (60 °C heating) of PSCs. Adapted with permission.^[62] Copyright 2020, Wiley. C) Schematic diagrams of the fabrication process for gradient grain-sized (GGS) CsPbI₃ films. Adapted with permission.^[61] Copyright 2020, Wiley. D) Stability under ambient environment (RH ≈ 20%; insets are the images of fresh and aged PSCs) for the different CsPbI₃ PSCs (TGS and LGS stand for tiny grain-sized and large grain-sized, respectively). Reproduced with permission.^[61] Copyright 2020, Wiley.

and methylammonium lead iodide (MAPI)-based devices (Figure 8B).^[62] Follow-up works applied the ADMA-assisted grain growth control to create a hierarchical morphology for the perovskite layer. In particular, a gradient grain-sized (GGS) structure has been created, with large grains on the bottom and tiny grains on top (Figure 8C). This GGS CsPbI₃ bilayer showed increased hydrophobicity, reduced trap-states, and nonradiative recombination.^[61] Finally, PSCs created with this method retained 85% of their initial PCE after 1000 h storage in ambient conditions (Figure 8D).^[61] Ye et al. have proposed an inorganic shunt-blocking LiF layer at the ETL/CsPbI_{3-x}Br_x interface, aiming to suppress the recombination losses through the optimization of the energy level alignment.^[60] Furthermore, a small amount of lead chloride has been added in the perovskite

precursors solution in order to modify the crystallization rate of the perovskite and obtain large grains with less grain boundaries. The incorporation of Cl⁻ into the perovskite lattice increases the value of the Goldsmith tolerance factor, thus increasing the stability of the photoactive phase.^[60] As a consequence of this double approach, the authors achieved a PCE of 18.64% in n-i-p configuration (Figure 9A), which was retained over 94% after 1000 h of light soaking in N₂ glovebox (Figure 9B).^[60]

Based on our literature research, most of the Cs-based all-inorganic PSCs are realized with an n-i-p structure. However, n-i-p structures made with spiro-OMeTAD as HTL need additional dopants such as 4-terbutylpyridine and hygroscopic lithium salts, which are believed to be one of the causes of degradation for PSCs.^[8] Despite n-i-p configuration being the

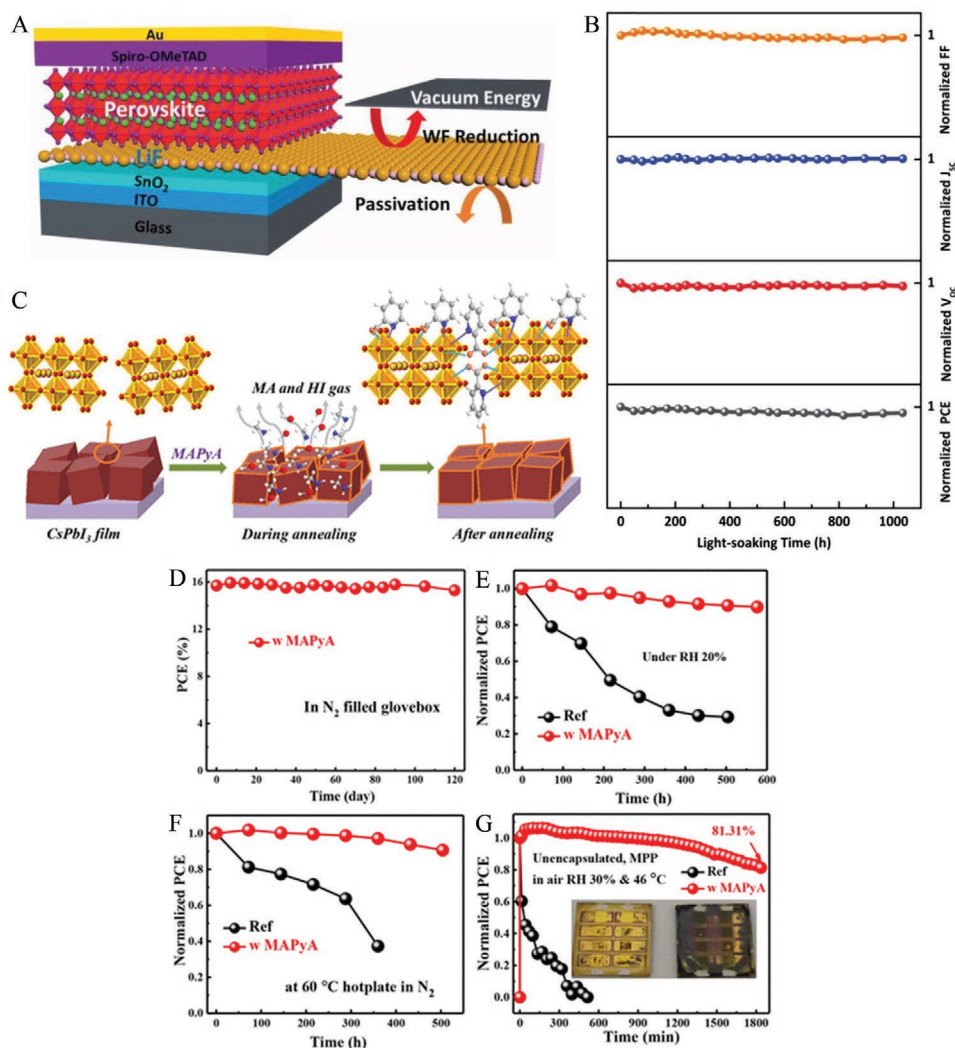


Figure 9. A) Schematic device architecture of the inorganic PSC; LiF was used to modify the SnO₂ surface. Adapted with permission.^[60] Copyright 2019, Wiley. B) Photostability of CsPbI_{3-x}Br_x with LiF interlayer and PbCl₂ additive; the stability was tested under continuous white LED illumination (100 mW cm⁻²) in a nitrogen glovebox without encapsulation. Adapted with permission.^[60] Copyright 2019, Wiley. C) Schematic of effects of MAPyA treatment on CsPbI₃ films. Reproduced with permission.^[51] Copyright 2020, American Chemical Society. D) Stability of devices stored in the N₂ filled glovebox for 120 days. Reproduced with permission.^[51] Copyright 2020, American Chemical Society. E,F) Moisture and thermal stabilities of the corresponding devices. Reproduced with permission.^[51] Copyright 2020, American Chemical Society. G) MPP tracking under RH 30% ambient condition with 100 mW cm⁻² LED-array illuminated at 46 °C, and the inset images are the photographs of the aged ref and MAPyA-treated devices. Adapted with permission.^[51] Copyright 2020, American Chemical Society.

most used for all-inorganic high efficiency solar cells, some research groups have decided to realize inverted p-i-n structures. Fu et al. reported the use of methylammonium pyridine-2-carboxylic salt (MAPyA) as a novel post-treatment agent for in situ healing and passivation of inverted CsPbI₃-based PSCs.^[51] During the annealing process, the MAPyA decomposes into methylamine gas and solid pyridine-2-carboxylic acid: while the first provides healing for nondense CsPbI₃, the latter can act as a barrier toward moisture erosion while stabilizing the photoactive phase through strong ionic interactions with the PbI₆ octahedra (Figure 9C).^[51] The optimized device revealed a PCE of 16.67%, which is among the highest reported for inverted p-i-n structures. Furthermore, the unencapsulated device features long-term stability when stored in a N₂ glovebox for 120 days

(Figure 9D) and it also showed great moisture and heat resistance, retaining the 89.7% of its PCE after aging at 20% RH for 526 h and 90.6% of the initial PCE after aging for 504 h at 60 °C (Figure 9E,F). Finally, the authors have conducted a MPP tracking experiment, where the devices were tested at 30% RH ambient condition and 46 °C with 100 mW cm⁻² LED illumination. The MAPyA-treated device retained 81.3% of its efficiency after 1800 min, compared to a retained PCE of 27% after 98 min of the reference cell, thus achieving long-term operational stability in ambient condition (Figure 9G).^[51] In conclusion, **Table 1** summarizes the most recent progresses in the field of all-inorganic Cs-based PSCs, reporting the active layer material, the device structure, the optimization strategy, the device area, and the PCE achieved.

Table 1. Main parameters of all-inorganic Cs-based perovskite solar cells.

Active material	Device structure	Optimization strategy	Device area [cm ²]	PCE [%]	Year	Refs.
CsPbI ₃	FTO/c-TiO ₂ /pero/spiro-oMeTAD/Au	HI additive	n.d.	2.90	2015	[19]
CsPbI ₃	FTO/c-TiO ₂ /pero/spiro-oMeTAD/Ag	Quasi-2D dimensionality reduction	0.12	11.86	2017	[49]
CsPbI ₃	FTO/c-TiO ₂ /pero/spiro-oMeTAD/Ag	Surface passivation with PTABr	0.12	17.06	2018	[45]
CsPbI ₃	FTO/c-TiO ₂ /pero/spiro-oMeTAD/Ag	Precursor engineering with DMAI Surface passivation with PTACl	0.1	19.03	2019	[15]
CsPbI ₃	FTO/c-TiO ₂ /pero/spiro-oMeTAD/Ag	Precursor engineering with DMAI Perovskite passivation with CHI	0.1	18.40	2019	[21]
CsPbI ₃	FTO/PTAA/pero/PCBM/BCP/Ag	Precursor engineering with organic terminal groups	0.09	13.32	2019	[50]
CsPbI _{3-x} Br _x	ITO/SnO ₂ /LiF/pero/spiro-oMeTAD/Au	Interface engineering with LiF Anion doping with PbCl ₂	0.07	18.64	2019	[60]
CsPbI ₃	FTO/c-TiO ₂ /pero/spiro-oMeTAD/MoO ₃ /Au	Precursor engineering with ABA Surface passivation with NGBr	0.12	18.27	2020	[43]
CsPbI ₃	ITO/SnO ₂ /pero/spiro-oMeTAD/Au	Interface engineering with Zn(C ₆ F ₅) ₂	0.09	19.00	2020	[44]
CsPbI ₂ Br	FTO/c-TiO ₂ /pero/P3HT/Ag	Surface passivation with Pb(DTTC) ₂	0.06	17.03	2020	[46]
CsPbI ₂ Br _{3-x}	ITO/SnO ₂ /pero/SIM/spiro-oMeTAD/Au	2D/3D interface engineering with GABr	0.1	18.06	2020	[47]
CsPbI ₃	FTO/c-TiO ₂ /pero/PTAA/Au	2D/3D interface engineering with GABr	n.d.	18.02	2020	[48]
CsPbI ₃	ITO/P3CT-N/pero/PCBM/C ₆₀ /BCP/Ag	Perovskite post-treatment with MAPyA	0.09	16.67	2020	[51]
CsPbI ₃	FTO/ZnO–ZnS/m-TiO ₂ /pero/spiro-oMeTAD/Au	Surface passivation with 18-crown-6 ether	0.1	16.90	2020	[17]
CsPbI ₂ Br	FTO/c-TiO ₂ /pero/spiro-oMeTAD/Au	B-site and X-site doping with CaCl ₂	0.09	16.79	2020	[58]
CsPbI ₃	FTO/c-TiO ₂ /pero/PTAA/Au	B-site doping with MnI ₂	n.d.	16.52	2020	[59]
CsPbI ₃	FTO/c-TiO ₂ /pero/spiro-oMeTAD/Au	Soft template-controlled crystal growth with ADMA	0.09	15.48	2020	[61]
CsPbI ₃	FTO/c-TiO ₂ /pero/spiro-oMeTAD/Au	Soft template-controlled crystal growth with ADMA	0.09	16.04	2020	[62]

4. Industrial Perspectives for All-Inorganic Perovskites

4.1. General Consideration on Perovskite Solar Cells Scale-Up

Although PSCs have achieved remarkable efficiencies and improved stability at the laboratory scale, a significant performance gap still exists with large area modules. To date, the highest reported certified efficiency is 17.9% for a 800 cm² module,^[63] about 70% than that of the champion cell.^[1]

The scale up from small-area cells to large-area modules implies a change of paradigm.^[64] Working on laboratory scale, there are factors that do not need imposed limitations in the search of higher PCE values. For instance, the viscosity of the solution does not need a strict control,^[64–67] toxic solvents can be safely used in a fume hood or in a glovebox; thermal treatments duration can span from minutes to hours without problems;^[64–67] the two steps sequential deposition is a commonly used approach; since glass supports can be used, the temperature of the treatment can be adjusted as desired.^[64–67] Furthermore, operations are often carried out in inert atmosphere and electrodes are frequently deposited through vacuum-assisted methods.

Similarly to organic photovoltaics, roll-to-roll (R2R) printing/coating techniques have the greatest potential to enable PSC scale-up at high throughput, but also pose inherent challenges.^[68,69] The R2R printing fabrication process developed for polymeric solar cells can be applied to perovskites under appropriate conditions.^[70,71] One focal point

is to identify the printing inks viscosity to obtain uniform and compact perovskite layers. The ideal printing conditions can be reached by identifying the correct combination of solvent and additives to be used in the ink formulation and their concentration, which can vary with the specific type of perovskite.^[72] Moreover, due to the different characteristics of inks for spin coating and for techniques like slot die coating,^[73–76] gravure printing,^[77,78] spray coating,^[79] ink-jet printing,^[80] or blade coating,^[81,82] much of the work devoted to optimizing the formulation cannot be directly applied to scaled-up production without reoptimization.

Another key point to consider is represented by the solvents used for the synthesis. Generally, the number of good solvents for perovskites is limited and most of them are hazardous and have high boiling point.^[83] Without safer alternatives, a scale-up of the technology is still technically possible. However, more strict security procedures would be necessary, leading to an inevitable increase of costs. In this context, a preliminary selection of innovative mixtures of solvents, which can match both the volatility and safety requirements can be carried out at first stage by the Hansen solubility parameters (HSP) approach.^[83,84] In this way, the HSP of solvent mixtures can be calculated and compared to HSP of perovskite precursors and charge transporting materials, so as to reduce the amount of solubility tests.

Reducing the processing time while maintaining the high quality of perovskite crystallization also represents a major point during the scale-up process. In this case, further studies are required to speed up the printing and annealing steps, necessary to get the right micro/macrosopic perovskite grain

morphology. The higher tolerance of inorganic perovskite to environmental agents with respect to hybrid perovskites can help to shift the fabrication of large-area devices from controlled to ambient conditions.^[13] However, further investigation is necessary to find the conditions to get pinhole-free, large grain size, and flat all-inorganic perovskite films with fast, one-step, and low temperature procedures.^[61,85–87]

Finally, the selection of interlayers as well as electrode materials is also critical in order to get full compatibility with the printing process without damaging the perovskite layer. To date, carbon-based electrodes are under study as substitutes of noble metal electrodes in order to have fully printable devices,^[88] such as HTL-free PSCs.^[89]

It is worth mentioning that the modules reported in the literature do not necessarily imply a fabrication with scalable, roll-to-roll compatible methods and that high PCE are often obtained when off-line steps are included.^[77,90] Moreover, to date, there is no evidence of R2R-printed all-inorganic PSCs in literature, but different efforts are present to reach the conditions for high-efficiency and stable solar cells made by this fabrication technique.^[91,92]

4.2. All-Inorganic Perovskite Solar Modules

The issues related to all-inorganic perovskites are even more fundamental to be addressed when large-area devices are fabricated. Even when a suitable scalable deposition technique is identified, the enlargement of the active area and the connection of different subcells in a module lead to inevitable efficiency loss due to increase of materials defects, geometrical factors, and electrical connections.^[64] In front of this performance losses, higher quality and stability of materials is required in order to get devices suitable for marketable applications.

The passivation of the perovskite and the charge transporting layers and the use of additives into the ink formulations represent two valid strategies for increasing both the quality and the stability of the thin films. For example, doping the C_{60} layer of a $ZnO@C_{60}$ electron-transporting-bilayer with tris(pentafluorophenyl)borane and $LiClO_4$ lead to reduced charge recombination and increased film conductivity.^[41] Applying this method, a 4 subcells spin-coated module with active area of 10.92 cm^2 achieved PCE of 12.19% (Figure 10A,B).^[41] However, the compatibility of this approach with scalable deposition methods is still to be proven. As reported above, 18-crown-6 ether is used to passivate and stabilize α - $CsPbI_3$ perovskite.^[17] The resulting films exhibit stronger resistance to moisture and reduction of surface defects. Moreover, 4 subcells modules deposited by spin coater achieved PCE = 11.87% (8 cm^2 active area), which maintained the 95.2% of the initial value after 500 h at MPP under continuous sun irradiation (RH = 60%, encapsulated) (Figures 7E and 10C,D).^[17] In another work, a 16 cm^2 module is fabricated by blade coating method modified with a vacuum-flash process, gaining PCE $\approx 10\%$.^[17] Unfortunately, the presence of a vacuum system, together with long annealing time, makes this method not compatible with industrial processes. An interesting solution to match commercial requirements can be represented by fast IR annealing systems.^[93]

In order to obtain commercial devices, the study of new material formulations for inorganic PSCs should progress together with the implementation of scalable techniques. The addition of $Zn(C_6F_5)_2$ in $CsPbI_3$ helped to obtain high-quality perovskite layer with fast blade-coating deposition at low temperature ($\leq 100\text{ }^\circ\text{C}$) in ambient condition.^[44] In this case, the obtained devices have small area (0.09 cm^2 , with best PCE = 19%) and, again, thermal treatment times of several minutes are exceedingly long for a high throughput process. The deposition of composition-graded $CsPbI_2Br$ thin film through spray-coating represents one of the most recent examples of large-area inorganic-perovskite-based device.^[94] The graded perovskite structure widens the absorption range and carrier lifetime and increases the efficiency of charge separation and collection.^[94] By this technique, a monolithically integrated module is obtained, with PCE = 13.82% (112 cm^2 aperture area) and $\approx 9\%$ degradation over 1000 h continuous 1 sun light soaking (Figure 10E,F).^[94] To summarize, Table 2 reports the most recent progresses in the field of all-inorganic Cs-based perovskite solar modules, showing the active layer material, the device structure, the optimization strategy, the deposition method, the device area, and the PCE achieved.

5. Concluding Remarks and Future Perspectives

Thanks to their remarkable thermal stability due to the absence of the hygroscopic organic cations, all-inorganic Cs-based PSCs have now been recognized as one of the most promising solution within the class of hybrid halide PSCs.^[2] This is further confirmed by the increased interest upon this class of materials, which led to a rapid PCE growth to over 19% in 2020.^[15] Nevertheless, several challenges are still to be coped with. For instance, the degradation of $CsPbI_3$ upon operation in ambient atmosphere still represents a major limit toward their marketable application. Furthermore, the PCE of all-inorganic PSCs are still lower compared to organic–inorganic counterpart, and they are still far from the Shockley–Queisser limit.^[2,16] Although many different strategies have been developed to deal with those issues, there is still a lot of work to be done in this field of research. For instance, an innovative approach can be represented by the deposition of lower-dimensional perovskites at the interface between the 3D perovskite and the selective charge transporting layers. Despite this has been mainly adopted for organic–inorganic hybrid perovskites,^[55,56] in the latest years, an interest toward this strategy has also been developed in the all-inorganic PSCs area, showing very promising results in terms of PCE and stability of the PSCs toward moisture and air.^[42,47,95,96] Alongside more common doping strategies in all-inorganic perovskite,^[42,59] pseudohalide doping on the X site and rubidium doping on the A site represent recently growing approaches, which in the near future may lead the path toward more efficient and stable all-inorganic PSCs.^[95,97] Finally, the possibility to realize fully all-inorganic perovskite solar cells, in which also the charge transporting layers are inorganic materials, may represent a promising pathway toward further increase the long term stability.^[41]

Further efforts are therefore required for the scale-up of all-inorganic Cs-based perovskites from laboratory-scale devices

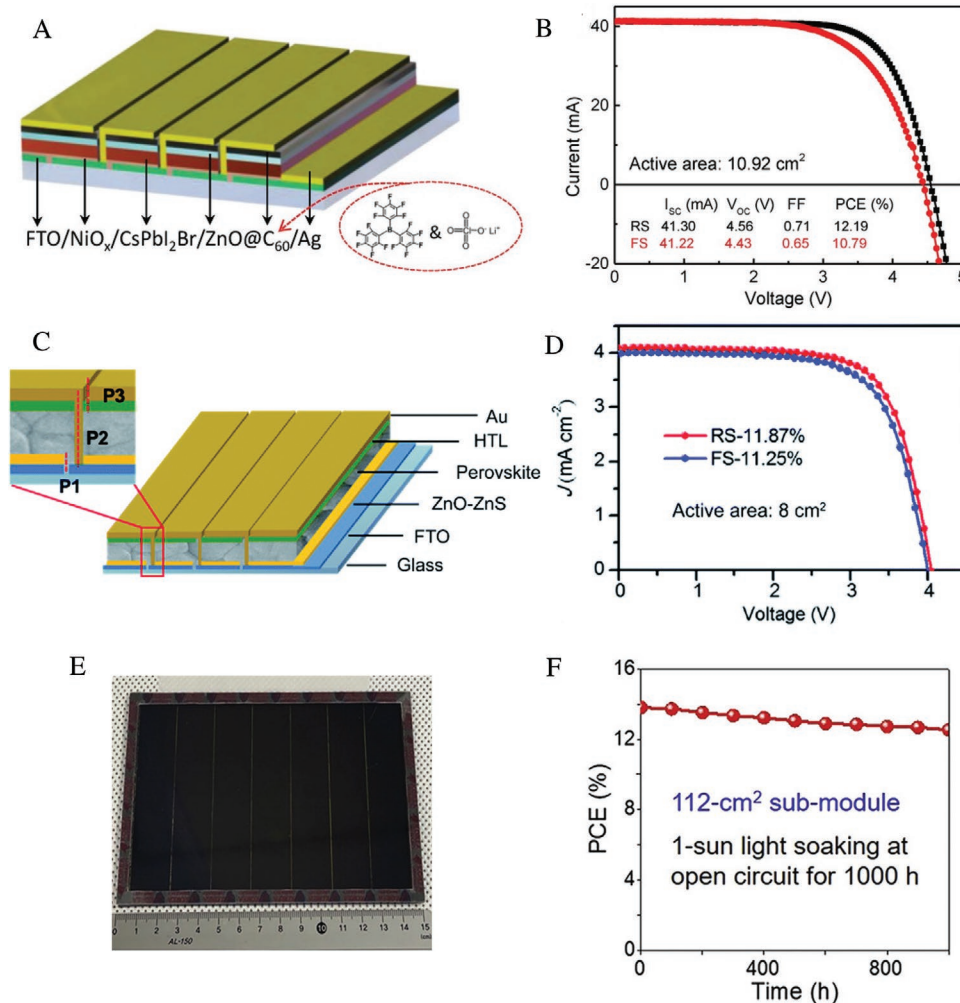


Figure 10. A) Schematic diagram of the perovskite solar module with four subcells connected in series. Reproduced with permission.^[41] Copyright 2020, Wiley. B) J - V characteristic curve of the best performing all-inorganic perovskite solar module. Reproduced with permission.^[41] Copyright 2020, Wiley. C) Schematic illustration of the perovskite solar module with inset showing the series connection regions. Reproduced with permission.^[17] Copyright 2020, Royal Society of Chemistry. D) J - V curves of the best performing CsPbI₃-Crown-based perovskite solar module. Reproduced with permission.^[17] Copyright 2020, Royal Society of Chemistry. E) Photographic image of the monolithically integrated perovskite solar module. Adapted with permission.^[94] Copyright 2020, Elsevier. F) Photostability of the monolithically integrated perovskite solar module under 1 sun light soaking. Adapted with permission.^[94] Copyright 2020, Elsevier.

Table 2. Main parameters of all-inorganic Cs-based perovskite solar modules.

Active material	Device structure	Optimization strategy	Deposition method	Device area [cm ²]	PCE [%]	Year	Refs.
CsPbI _x Br _{3-x}	FTO/c-TiO ₂ /pero/spiro-oMeTAD/Ag	Quasi-2D dimensionality reduction	Blade coating + vacuum-flash annealing	16	10.30	2018	[93]
CsPbI ₂ Br	FTO/NiO _x /pero/ZnO@C ₆₀ /Ag	Doping C ₆₀ with tris(pentafluorophenyl) borane and LiClO ₄	"Quasi-curved" heating	10.92	12.19	2020	[41]
CsPbI ₃	FTO/ZnO-ZnS/m-TiO ₂ /pero/spiro-oMeTAD/Au	Surface passivation with 18-crown-6 ether	Spin coating	8	11.87	2020	[17]
CsPbI ₃	FTO/ZnO-ZnS/m-TiO ₂ /pero/spiro-oMeTAD/Au	Surface passivation with 18-crown-6 ether	Blade coating	8	10.73	2020	[17]
CsPbI _{3-x} Br _x	FTO/TiO ₂ /pero/PTAA/Au	Graded Br-doping structure	Spray coating	112	13.82	2020	[94]

to marketable modules. As mentioned in the previous section, the fundamental issues of CsPbI₃ are magnified during the scale-up process. For instance, the need to maintain high uniformities even with large active areas is one of the major concerns.^[44] Furthermore, the more severe restrictions introduced by roll-to-roll printing/coating techniques greatly increase the difficulty of the challenge.^[72] Nevertheless, several promising results were achieved in 2020, with a record efficiency of 13.82% for a 112 cm² submodule.^[94] In addition, several research groups are now focusing their efforts toward the realization of all-inorganic Cs-based PSCs with scalable techniques, thus achieving 19% PCE in 2020 via blade coating deposition.^[44]

When considering potential commercial applications, CsPbI₃ can be successfully employed in single junction solar cells, delivering moderately high efficiency (>19%) devices with good stability, despite much work has still to be done to reach the performances of common organic–inorganic hybrid perovskites—nowadays 25.6%^[98]—and the stability standards imposed by the market. Alternatively, all-inorganic single junction solar cells, for instance, in the p–i–n configuration, can be ideally adopted in tandem devices, where the perovskite cell is engineered on top of standard inorganic Si or CIGS cells, but also on perovskites forming all perovskite tandem junctions.^[99] CsPbI₃ is particularly suitable for its bandgap as top subcell in a two-terminal configuration, as also confirmed from theoretical calculations.^[100] However, experimental works on tandem devices comprising all-inorganic perovskites are quite scarce.^[100–102] This is mainly due to the intrinsic instability of the CsPbI₃ active layer,^[100,103] which still limits its successful implementation in tandem configuration. However, the methods aiming to increase the Goldsmith tolerance factor to improve the stability of the CsPbI₃ photoactive phase discussed in the review can be easily translated from single junction device optimization to tandem structures, encouraging timely improvements of CsPbI₃ tandem devices. In particular, among the few works reported, an interesting application of CsPbI₃ in tandem devices is represented by all-inorganic perovskite/organic tandem solar cells, which have achieved 18% PCE in 2020.^[103] On the other side, perovskite/perovskite tandem devices offer the potential to be an interesting technology due to their lightweight, spectral tunability, and low costs. In this regard, material fabrication, morphology optimization, and stabilization are still far to be optimized, limiting their development.^[99,103] For instance, common solvents such as dimethylformamide and dimethyl sulfoxide can penetrate through the interconnection junction (ICJ) and severely damage the bottom perovskite film.^[103] This calls for intense research in this direction, for instance, in the development of different ICJs, such as thick indium tin oxide films,^[104] to offer new potential solutions for the fabrication of all-perovskite tandem solar cells.^[104,105]

Alongside classic power generation, all-inorganic perovskites can promisingly be employed in portable devices, fulfilling new modern needs, for instance, in the IoT field. In fact, their suitability to be printed on flexible substrates, in air, along with their tunable bandgap make these materials an appealing technology to face the new market segments asking for adaptable and flexible devices, where Si solar panels fail.^[106]

To summarize, in this review, we have analyzed the all-inorganic Cs-based perovskites, starting from the material

structural and optical properties, we have reviewed the most common processes for the deposition of highly crystalline thin films, and we have discussed the applications in PSCs, including the most recent and noticeable efforts made to increase both the PCE and the stability of the solar cells up to now. Finally, we discussed the potential implications for the scale-up of this technology, analyzing the scaling-up challenges and reporting the most advanced works in this field. Although there is still a long way to go and several challenges to be dealt with, all-inorganic Cs-based perovskites pave the way for promising candidate for next-generation efficient and stable perovskite photovoltaics. In addition, it is worth noticing that all-inorganic single junction devices offer interesting potential applications in high impact optoelectronics. Examples include photodetectors for gamma and X-rays detection,^[107–111] scintillators,^[112–115] photocatalysts,^[116–119] and light emitting devices,^[120–123] offering a plethora of new attractive solutions.

Acknowledgements

G.G. acknowledges the “HY-NANO” project that has received funding from the European Research Council (ERC) Starting Grant 2018 under the European Union’s Horizon 2020 research and innovation programme (grant agreement no. 802862). R.M. and G.G. acknowledge the Ph.D. Fellowship from Eni S.p.A. G.G. acknowledges the project Cariplo Economia Circolare 2021 FLHYPER (no. 2020-1067).

Conflict of Interest

The authors declare no conflict of interest.

Keywords

all-inorganic perovskites, perovskite solar cells, upscaling

Received: February 25, 2021

Revised: April 9, 2021

Published online:

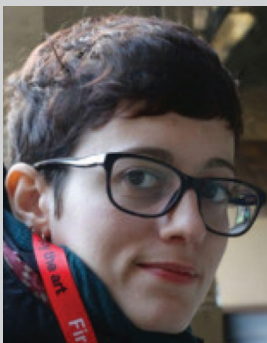
- [1] Best Research-Cell Efficiency Chart, <https://www.nrel.gov/pv/cell-efficiency.html> (accessed: December 2020).
- [2] J. Tian, Q. Xue, Q. Yao, N. Li, C. J. Brabec, H. Yip, *Adv. Energy Mater.* **2020**, *10*, 2000183.
- [3] M. Saliba, J.-P. Correa-Baena, M. Grätzel, A. Hagfeldt, A. Abate, *Angew. Chem., Int. Ed.* **2018**, *57*, 2554.
- [4] K. X. Steirer, P. Schulz, G. Teeter, V. Stevanovic, M. Yang, K. Zhu, J. J. Berry, *ACS Energy Lett.* **2016**, *1*, 360.
- [5] X. Dai, Y. Deng, C. H. Van Brackle, S. Chen, P. N. Rudd, X. Xiao, Y. Lin, B. Chen, J. Huang, *Adv. Energy Mater.* **2020**, *10*, 1903108.
- [6] X. Meng, Z. Cai, Y. Zhang, X. Hu, Z. Xing, Z. Huang, Z. Huang, Y. Cui, T. Hu, M. Su, X. Liao, L. Zhang, F. Wang, Y. Song, Y. Chen, *Nat. Commun.* **2020**, *11*, 3016.
- [7] Q. Tai, K.-C. Tang, F. Yan, *Energy Environ. Sci.* **2019**, *12*, 2375.
- [8] G. Schileo, G. Grancini, *J. Phys.: Energy* **2020**, *2*, 021005.
- [9] N. Aristidou, I. Sanchez-Molina, T. Chotchuangchuchaval, M. Brown, L. Martinez, T. Rath, S. A. Haque, *Angew. Chem., Int. Ed.* **2015**, *54*, 8208.
- [10] S.-W. Lee, S. Kim, S. Bae, K. Cho, T. Chung, L. E. Mundt, S. Lee, S. Park, H. Park, M. C. Schubert, S. W. Glunz, Y. Ko, Y. Jun, Y. Kang, H.-S. Lee, D. Kim, *Sci. Rep.* **2016**, *6*, 38150.

- [11] B. Conings, J. Drijkoningen, N. Gauquelin, A. Babayigit, J. D'Haen, L. D'Olieslaeger, A. Ethirajan, J. Verbeeck, J. Manca, E. Mosconi, F. D. Angelis, H.-G. Boyen, *Adv. Energy Mater.* **2015**, *5*, 1500477.
- [12] P. Toloueinia, H. Khassaf, A. Shirazi Amin, Z. M. Tobin, S. P. Alpay, S. L. Suib, *ACS Appl. Energy Mater.* **2020**, *3*, 8240.
- [13] M. Kulbak, S. Gupta, N. Kedem, I. Levine, T. Bendikov, G. Hodes, D. Cahen, *J. Phys. Chem. Lett.* **2016**, *7*, 167.
- [14] E. Tenuta, C. Zheng, O. Rubel, *Sci. Rep.* **2016**, *6*, 37654.
- [15] Y. Wang, X. Liu, T. Zhang, X. Wang, M. Kan, J. Shi, Y. Zhao, *Angew. Chem., Int. Ed.* **2019**, *58*, 16691.
- [16] S. Rühle, *Sol. Energy* **2016**, *130*, 139.
- [17] R. Chen, Y. Hui, B. Wu, Y. Wang, X. Huang, Z. Xu, P. Ruan, W. Zhang, F. Cheng, W. Zhang, J. Yin, J. Li, N. Zheng, *J. Mater. Chem. A* **2020**, *8*, 9597.
- [18] A. Marronnier, G. Roma, S. Boyer-Richard, L. Pedesseau, J.-M. Jancu, Y. Bonnassieux, C. Katan, C. C. Stoumpos, M. G. Kanatzidis, J. Even, *ACS Nano* **2018**, *12*, 3477.
- [19] G. E. Eperon, G. M. Paternò, R. J. Sutton, A. Zampetti, A. A. Haghighirad, F. Cacialli, H. J. Snaith, *J. Mater. Chem. A* **2015**, *3*, 19688.
- [20] R. J. Sutton, M. R. Filip, A. A. Haghighirad, N. Sakai, B. Wenger, F. Giustino, H. J. Snaith, *ACS Energy Lett.* **2018**, *3*, 1787.
- [21] Y. Wang, M. I. Dar, L. K. Ono, T. Zhang, M. Kan, Y. Li, L. Zhang, X. Wang, Y. Yang, X. Gao, Y. Qi, M. Grätzel, Y. Zhao, *Science* **2019**, *365*, 591.
- [22] M. Kulbak, D. Cahen, G. Hodes, *J. Phys. Chem. Lett.* **2015**, *6*, 2452.
- [23] A. Swarnkar, W. J. Mir, A. Nag, *ACS Energy Lett.* **2018**, *3*, 286.
- [24] G. Tong, L. K. Ono, Y. Qi, *Energy Technol.* **2020**, *8*, 1900961.
- [25] G. Tong, T. Chen, H. Li, W. Song, Y. Chang, J. Liu, L. Yu, J. Xu, Y. Qi, Y. Jiang, *Sol. RRL* **2019**, *3*, 1900030.
- [26] T. Xiang, Y. Zhang, H. Wu, J. Li, L. Yang, K. Wang, J. Xia, Z. Deng, J. Xiao, W. Li, Z. Ku, F. Huang, J. Zhong, Y. Peng, Y.-B. Cheng, *Sol. Energy Mater. Sol. Cells* **2020**, *206*, 110317.
- [27] G. Tong, T. Chen, H. Li, L. Qiu, Z. Liu, Y. Dang, W. Song, L. K. Ono, Y. Jiang, Y. Qi, *Nano Energy* **2019**, *65*, 104015.
- [28] Y. Rakita, N. Kedem, S. Gupta, A. Sadhanala, V. Kalchenko, M. L. Böhm, M. Kulbak, R. H. Friend, D. Cahen, G. Hodes, *Cryst. Growth Des.* **2016**, *16*, 5717.
- [29] S. Caicedo-Dávila, H. Funk, R. Lovrinčić, C. Müller, M. Sendner, O. Cojocar-Mirédin, F. Lehmann, R. Gunder, A. Franz, S. Levenco, A. V. Cohen, L. Kronik, B. Haas, C. T. Koch, D. Abou-Ras, *J. Phys. Chem. C* **2019**, *123*, 17666.
- [30] M. Liu, J. Zhao, Z. Luo, Z. Sun, N. Pan, H. Ding, X. Wang, *Chem. Mater.* **2018**, *30*, 5846.
- [31] J. Feng, X. Han, H. Huang, Q. Meng, Z. Zhu, T. Yu, Z. Li, Z. Zou, *Sci. Bull.* **2020**, *65*, 726.
- [32] R. J. Sutton, G. E. Eperon, L. Miranda, E. S. Parrott, B. A. Kamino, J. B. Patel, M. T. Hörlantner, M. B. Johnston, A. A. Haghighirad, D. T. Moore, H. J. Snaith, *Adv. Energy Mater.* **2016**, *6*, 1502458.
- [33] W. Zhou, Y. Zhao, X. Zhou, R. Fu, Q. Li, Y. Zhao, K. Liu, D. Yu, Q. Zhao, *J. Phys. Chem. Lett.* **2017**, *8*, 4122.
- [34] E. T. Hoke, D. J. Slotcavage, E. R. Dohner, A. R. Bowring, H. I. Karunadasa, M. D. McGehee, *Chem. Sci.* **2015**, *6*, 613.
- [35] R. E. Beal, D. J. Slotcavage, T. Leijtens, A. R. Bowring, R. A. Belisle, W. H. Nguyen, G. F. Burkhard, E. T. Hoke, M. D. McGehee, *J. Phys. Chem. Lett.* **2016**, *7*, 746.
- [36] P. Luo, Y. Zhou, W. Xia, S. Zhou, J. Liu, Y. Lu, C. Xu, L. Sun, *Ceram. Int.* **2018**, *44*, 12783.
- [37] Z.-L. Yu, Y.-Q. Zhao, Q. Wan, B. Liu, J.-L. Yang, M.-Q. Cai, *J. Phys. Chem. C* **2020**, *124*, 23052.
- [38] J. Kang, L.-W. Wang, *J. Phys. Chem. Lett.* **2017**, *8*, 489.
- [39] D. W. deQuilettes, K. Frohna, D. Emin, T. Kirchartz, V. Bulovic, D. S. Ginger, S. D. Stranks, *Chem. Rev.* **2019**, *119*, 11007.
- [40] T. Leijtens, G. E. Eperon, A. J. Barker, G. Grancini, W. Zhang, J. M. Ball, A. R. Srimath Kandada, H. J. Snaith, A. Petrozza, *Energy Environ. Sci.* **2016**, *9*, 3472.
- [41] C. Liu, Y. Yang, C. Zhang, S. Wu, L. Wei, F. Guo, G. M. Arumugam, J. Hu, X. Liu, J. Lin, R. E. I. Schropp, Y. Mai, *Adv. Mater.* **2020**, *32*, 1907361.
- [42] Z. Li, X. Liu, J. Xu, S. Yang, H. Zhao, H. Huang, S. F. Liu, J. Yao, *J. Phys. Chem. Lett.* **2020**, *11*, 4138.
- [43] Y. Wang, G. Chen, D. Ouyang, X. He, C. Li, R. Ma, W.-J. Yin, W. C. H. Choy, *Adv. Mater.* **2020**, *32*, 2000186.
- [44] X. Chang, J. Fang, Y. Fan, T. Luo, H. Su, Y. Zhang, J. Lu, L. Tsetseris, T. D. Anthopoulos, S. (F.) Liu, K. Zhao, *Adv. Mater.* **2020**, *32*, 2001243.
- [45] Y. Wang, T. Zhang, M. Kan, Y. Zhao, *J. Am. Chem. Soc.* **2018**, *140*, 12345.
- [46] J. He, J. Liu, Y. Hou, Y. Wang, S. Yang, H. G. Yang, *Nat. Commun.* **2020**, *11*, 4237.
- [47] Y. Zheng, X. Yang, R. Su, P. Wu, Q. Gong, R. Zhu, *Adv. Funct. Mater.* **2020**, *30*, 2000457.
- [48] C. Yan, Z. Li, Y. Sun, J. Zhao, X. Huang, J. Yang, Z. Ci, L. Ding, Z. Jin, *J. Mater. Chem. A* **2020**, *8*, 10346.
- [49] T. Zhang, M. I. Dar, G. Li, F. Xu, N. Guo, M. Grätzel, Y. Zhao, *Sci. Adv.* **2017**, *3*, e1700841.
- [50] T. Wu, Y. Wang, Z. Dai, D. Cui, T. Wang, X. Meng, E. Bi, X. Yang, L. Han, *Adv. Mater.* **2019**, *31*, 1900605.
- [51] S. Fu, L. Wan, W. Zhang, X. Li, W. Song, J. Fang, *ACS Energy Lett.* **2020**, *5*, 3314.
- [52] S. Zhang, S. Wu, W. Chen, H. Zhu, Z. Xiong, Z. Yang, C. Chen, R. Chen, L. Han, W. Chen, *Mater. Today Energy* **2018**, *8*, 125.
- [53] J. Wang, J. Zhang, Y. Zhou, H. Liu, Q. Xue, X. Li, C.-C. Chueh, H.-L. Yip, Z. Zhu, A. K. Y. Jen, *Nat. Commun.* **2020**, *11*, 177.
- [54] W. Ke, I. Spanopoulos, C. C. Stoumpos, M. G. Kanatzidis, *Nat. Commun.* **2018**, *9*, 4785.
- [55] G. Grancini, M. K. Nazeeruddin, *Nat. Rev. Mater.* **2019**, *4*, 4.
- [56] G. Grancini, C. Roldán-Carmona, I. Zimmermann, E. Mosconi, X. Lee, D. Martineau, S. Narbey, F. Oswald, F. De Angelis, M. Grätzel, M. K. Nazeeruddin, *Nat. Commun.* **2017**, *8*, 15684.
- [57] M. V. Kenkin, E. A. Katz, A. Abate, G. Bardizza, J. J. Berry, C. Brabec, F. Brunetti, V. Bulović, Q. Burlingame, A. Di Carlo, R. Cheacharoen, Y.-B. Cheng, A. Colmann, S. Cros, K. Domanski, M. Duszka, C. J. Fell, S. R. Forrest, Y. Galagan, D. Di Girolamo, M. Grätzel, A. Hagfeldt, E. von Hauff, H. Hoppe, J. Kettle, H. Köbler, M. S. Leite, S. (F.) Liu, Y.-L. Loo, J. M. Luther, C.-Q. Ma, M. Madsen, M. Manceau, M. Matheron, M. McGehee, R. Meitzner, M. K. Nazeeruddin, A. F. Nogueira, Ç. Odabaşı, A. Osherov, N.-G. Park, M. O. Reese, F. De Rossi, M. Saliba, U. S. Schubert, H. J. Snaith, S. D. Stranks, W. Tress, P. A. Troshin, V. Turkovic, S. Veenstra, I. Visoly-Fisher, A. Walsh, T. Watson, H. Xie, R. Yildirim, S. M. Zakeeruddin, K. Zhu, M. Lira-Cantu, *Nat. Energy* **2020**, *5*, 35.
- [58] Y. Han, H. Zhao, C. Duan, S. Yang, Z. Yang, Z. Liu, S. (F.) Liu, *Adv. Funct. Mater.* **2020**, *30*, 1909972.
- [59] Z. Yao, W. Zhao, S. Chen, Z. Jin, S. F. Liu, *ACS Appl. Energy Mater.* **2020**, *3*, 5190.
- [60] Q. Ye, Y. Zhao, S. Mu, F. Ma, F. Gao, Z. Chu, Z. Yin, P. Gao, X. Zhang, J. You, *Adv. Mater.* **2019**, *31*, 1905143.
- [61] C. Liu, Y. Yang, O. A. Syzgantseva, Y. Ding, M. A. Syzgantseva, X. Zhang, A. M. Asiri, S. Dai, M. K. Nazeeruddin, *Adv. Mater.* **2020**, *32*, 2002632.
- [62] C. Liu, Y. Yang, X. Xia, Y. Ding, Z. Arain, S. An, X. Liu, R. C. Cristina, S. Dai, M. K. Nazeeruddin, *Adv. Energy Mater.* **2020**, *10*, 1903751.
- [63] Champion Photovoltaic Module Efficiency Chart, <https://www.nrel.gov/pv/module-efficiency.html> (accessed: December 2020).
- [64] Z. Li, T. R. Klein, D. H. Kim, M. Yang, J. J. Berry, M. F. A. M. van Hest, K. Zhu, *Nat. Rev. Mater.* **2018**, *3*, 18017.
- [65] N.-G. Park, K. Zhu, *Nat. Rev. Mater.* **2020**, *5*, 333.
- [66] Y. Galagan, *J. Phys. Chem. Lett.* **2018**, *9*, 4326.
- [67] Y. Rong, Y. Ming, W. Ji, D. Li, A. Mei, Y. Hu, H. Han, *J. Phys. Chem. Lett.* **2018**, *9*, 2707.

- [68] R. Po, A. Bernardi, A. Calabrese, C. Carbonera, G. Corso, A. Pellegrino, *Energy Environ. Sci.* **2014**, *7*, 925.
- [69] S. T. Williams, A. Rajagopal, C.-C. Chueh, A. K.-Y. Jen, *J. Phys. Chem. Lett.* **2016**, *7*, 811.
- [70] F. C. Krebs, *Sol. Energy Mater. Sol. Cells* **2009**, *93*, 394.
- [71] X. Peng, J. Yuan, S. Shen, M. Gao, A. S. R. Chesman, H. Yin, J. Cheng, Q. Zhang, D. Angmo, *Adv. Funct. Mater.* **2017**, *27*, 1703704.
- [72] B. Dou, J. B. Whitaker, K. Bruening, D. T. Moore, L. M. Wheeler, J. Ryter, N. J. Breslin, J. J. Berry, S. M. Garner, F. S. Barnes, S. E. Shaheen, C. J. Tassone, K. Zhu, M. F. A. M. van Hest, *ACS Energy Lett.* **2018**, *3*, 2558.
- [73] Y. Galagan, F. D. Giacomo, H. Gorter, G. Kirchner, I. de Vries, R. Andriessen, P. Groen, *Adv. Energy Mater.* **2018**, *8*, 1801935.
- [74] T. M. Schmidt, T. T. Larsen-Olsen, J. E. Carlé, D. Angmo, F. C. Krebs, *Adv. Energy Mater.* **2015**, *5*, 1500569.
- [75] K. Hwang, Y.-S. Jung, Y.-J. Heo, F. H. Scholes, S. E. Watkins, J. Subbiah, D. J. Jones, D.-Y. Kim, D. Vak, *Adv. Mater.* **2015**, *27*, 1241.
- [76] D. Burkitt, R. Patidar, P. Greenwood, K. Hooper, J. McGettrick, S. Dimitrov, M. Colombo, V. Stoichkov, D. Richards, D. Beynon, M. Davies, T. Watson, *Sustainable Energy Fuels* **2020**, *4*, 3340.
- [77] Y. Y. Kim, T.-Y. Yang, R. Suhonen, M. Välimäki, T. Maaninen, A. Kemppainen, N. J. Jeon, J. Seo, *Adv. Sci.* **2019**, *6*, 1802094.
- [78] Y. Y. Kim, T.-Y. Yang, R. Suhonen, A. Kemppainen, K. Hwang, N. J. Jeon, J. Seo, *Nat. Commun.* **2020**, *11*, 5146.
- [79] S. Uličná, B. Dou, D. H. Kim, K. Zhu, J. M. Walls, J. W. Bowers, M. F. A. M. van Hest, *ACS Appl. Energy Mater.* **2018**, *1*, 1853.
- [80] F. Mathies, H. Eggers, B. S. Richards, G. Hernandez-Sosa, U. Lemmer, U. W. Paetzold, *ACS Appl. Energy Mater.* **2018**, *1*, 1834.
- [81] Z. Yang, C.-C. Chueh, F. Zuo, J. H. Kim, P.-W. Liang, A. K.-Y. Jen, *Adv. Energy Mater.* **2015**, *5*, 1500328.
- [82] Z. Ouyang, M. Yang, J. B. Whitaker, D. Li, M. F. A. M. van Hest, *ACS Appl. Energy Mater.* **2020**, *3*, 3714.
- [83] K. L. Gardner, J. G. Tait, T. Merckx, W. Qiu, U. W. Paetzold, L. Kootstra, M. Jaysankar, R. Gehlhaar, D. Cheyns, P. Heremans, J. Poortmans, *Adv. Energy Mater.* **2016**, *6*, 1600386.
- [84] X. Cao, G. Zhang, Y. Cai, L. Jiang, X. He, Q. Zeng, J. Wei, Y. Jia, G. Xing, W. Huang, *Sol. RRL* **2020**, *4*, 2000008.
- [85] X. Wang, X. Ran, X. Liu, H. Gu, S. Zuo, W. Hui, H. Lu, B. Sun, X. Gao, J. Zhang, Y. Xia, Y. Chen, W. Huang, *Angew. Chem., Int. Ed.* **2020**, *59*, 13354.
- [86] Z. Zhao, F. Gu, H. Rao, S. Ye, Z. Liu, Z. Bian, C. Huang, *Adv. Energy Mater.* **2019**, *9*, 1802671.
- [87] J. Ma, J. Su, Z. Lin, L. Zhou, J. He, J. Zhang, S. Liu, J. Chang, Y. Hao, *Nano Energy* **2020**, *67*, 104241.
- [88] Z. Liu, B. Sun, X. Liu, J. Han, H. Ye, T. Shi, Z. Tang, G. Liao, *Nano-Micro Lett.* **2018**, *10*, 34.
- [89] W. Zhu, Z. Zhang, W. Chai, D. Chen, H. Xi, J. Chang, J. Zhang, C. Zhang, Y. Hao, *ACS Appl. Energy Mater.* **2019**, *2*, 5254.
- [90] A. Priyadarshi, L. J. Haur, P. Murray, D. Fu, S. Kulkarni, G. Xing, T. C. Sum, N. Mathews, S. G. Mhaisalkar, *Energy Environ. Sci.* **2016**, *9*, 3687.
- [91] D. Huang, P. Xie, Z. Pan, H. Rao, X. Zhong, *J. Mater. Chem. A* **2019**, *7*, 22420.
- [92] J. Song, L. Xu, J. Li, J. Xue, Y. Dong, X. Li, H. Zeng, *Adv. Mater.* **2016**, *28*, 4861.
- [93] S. Sanchez, N. Christoph, B. Grobety, N. Phung, U. Steiner, M. Saliba, A. Abate, *Adv. Energy Mater.* **2018**, *8*, 1802060.
- [94] J. H. Heo, F. Zhang, C. Xiao, S. J. Heo, J. K. Park, J. J. Berry, K. Zhu, S. H. Im, *Joule* **2021**, *5*, 481.
- [95] W. Zhang, J. Xiong, J. Li, W. A. Daoud, *Sol. RRL* **2020**, *4*, 2000112.
- [96] K. Wang, Z. Li, F. Zhou, H. Wang, H. Bian, H. Zhang, Q. Wang, Z. Jin, L. Ding, S. (F.) Liu, *Adv. Energy Mater.* **2019**, *9*, 1902529.
- [97] Z. Yao, Z. Jin, X. Zhang, Q. Wang, H. Zhang, Z. Xu, L. Ding, S. (F.) Liu, *J. Mater. Chem. C* **2019**, *7*, 13736.
- [98] J. Jeong, M. Kim, J. Seo, H. Lu, P. Ahlawat, A. Mishra, Y. Yang, M. A. Hope, F. T. Eickemeyer, M. Kim, Y. J. Yoon, I. W. Choi, B. P. Darwich, S. J. Choi, Y. Jo, J. H. Lee, B. Walker, S. M. Zakeeruddin, L. Emsley, U. Rothlisberger, A. Hagfeldt, D. S. Kim, M. Grätzel, J. Y. Kim, *Nature* **2021**, *592*, 381.
- [99] M. Jošt, L. Kegelmann, L. Korte, S. Albrecht, *Adv. Energy Mater.* **2020**, *10*, 1904102.
- [100] L. Meng, Z. Wei, T. Zuo, P. Gao, *Nano Energy* **2020**, *75*, 104866.
- [101] W. Ahmad, J. Khan, G. Niu, J. Tang, *Sol. RRL* **2017**, *1*, 1700048.
- [102] K. Hamada, K. Yonezawa, K. Yamamoto, R. A. Taima, S. Hayase, N. Ooyagi, Y. Yamamoto, K. Ohdaira, *Jpn. J. Appl. Phys.* **2019**, *58*, SBBF06.
- [103] S. Xie, R. Xia, Z. Chen, J. Tian, L. Yan, M. Ren, Z. Li, G. Zhang, Q. Xue, H.-L. Yip, Y. Cao, *Nano Energy* **2020**, *78*, 105238.
- [104] G. E. Eperon, T. Leijtens, K. A. Bush, R. Prasanna, T. Green, J. T.-W. Wang, D. P. McMeekin, G. Volonakis, R. L. Milot, R. May, A. Palmstrom, D. J. Slotcavage, R. A. Belisle, J. B. Patel, E. S. Parrott, R. J. Sutton, W. Ma, F. Moghadam, B. Conings, A. Babayigit, H.-G. Boyen, S. Bent, F. Giustino, L. M. Herz, M. B. Johnston, M. D. McGehee, H. J. Snaith, *Science* **2016**, *354*, 861.
- [105] D. Forgács, L. Gil-Escrig, D. Pérez-Del-Rey, C. Momblona, J. Werner, B. Niesen, C. Ballif, M. Sessolo, H. J. Bolink, *Adv. Energy Mater.* **2017**, *7*, 1602121.
- [106] X. Yang, H. Yang, X. Hu, W. Li, Z. Fang, K. Zhang, R. Huang, J. Li, Z. Yang, Y. Song, *J. Mater. Chem. A* **2020**, *8*, 5308.
- [107] Y. He, C. C. Stoumpos, I. Hadar, Z. Luo, K. M. McCall, Z. Liu, D. Y. Chung, B. W. Wessels, M. G. Kanatzidis, *J. Am. Chem. Soc.* **2021**, *143*, 2068.
- [108] Y. He, M. Petryk, Z. Liu, D. G. Chica, I. Hadar, C. Leak, W. Ke, I. Spanopoulos, W. Lin, D. Y. Chung, B. W. Wessels, Z. He, M. G. Kanatzidis, *Nat. Photonics* **2021**, *15*, 36.
- [109] W. Zhu, M. Deng, D. Chen, Z. Zhang, W. Chai, D. Chen, H. Xi, J. Zhang, C. Zhang, Y. Hao, *ACS Appl. Mater. Interfaces* **2020**, *12*, 32961.
- [110] P. Gui, J. Li, X. Zheng, H. Wang, F. Yao, X. Hu, Y. Liu, G. Fang, *J. Mater. Chem. C* **2020**, *8*, 6804.
- [111] T. Yang, F. Li, R. Zheng, *ACS Appl. Electron. Mater.* **2019**, *1*, 1348.
- [112] Q. Chen, J. Wu, X. Ou, B. Huang, J. Almutlag, A. A. Zhumekenov, X. Guan, S. Han, L. Liang, Z. Yi, J. Li, X. Xie, Y. Wang, Y. Li, D. Fan, D. B. L. Teh, A. H. All, O. F. Mohammed, O. M. Bakr, T. Wu, M. Bettinelli, H. Yang, W. Huang, X. Liu, *Nature* **2018**, *561*, 88.
- [113] Q. Xu, J. Wang, W. Shao, X. Ouyang, X. Wang, X. Zhang, Y. Guo, X. Ouyang, *Nanoscale* **2020**, *12*, 9727.
- [114] L. Yang, H. Zhang, M. Zhou, L. Zhao, W. Chen, T. Wang, X. Yu, D. Zhou, J. Qiu, X. Xu, *J. Phys. Chem. Lett.* **2020**, *11*, 9203.
- [115] Z. Ji, G. Cen, C. Su, Y. Liu, Z. Zhao, C. Zhao, W. Mai, *Adv. Opt. Mater.* **2020**, *8*, 2001436.
- [116] Y.-F. Xu, M.-Z. Yang, B.-X. Chen, X.-D. Wang, H.-Y. Chen, D.-B. Kuang, C.-Y. Su, *J. Am. Chem. Soc.* **2017**, *139*, 5660.
- [117] J. Chen, C. Dong, H. Idriss, O. F. Mohammed, O. M. Bakr, *Adv. Energy Mater.* **2020**, *10*, 1902433.
- [118] I. Poli, U. Hintermair, M. Regue, S. Kumar, E. V. Sackville, J. Baker, T. M. Watson, S. Eslava, P. J. Cameron, *Nat. Commun.* **2019**, *10*, 2097.
- [119] X.-X. Guo, S.-F. Tang, Y.-F. Mu, L.-Y. Wu, G.-X. Dong, M. Zhang, *RSC Adv.* **2019**, *9*, 34342.
- [120] L. Bai, S. Wang, Y. Zhang, K. Zhang, H. Li, K. Ou, L. Yi, *J. Lumin.* **2020**, *226*, 117422.
- [121] J. K. Nam, S. U. Chai, W. Cha, Y. J. Choi, W. Kim, M. S. Jung, J. Kwon, D. Kim, J. H. Park, *Nano Lett.* **2017**, *17*, 2028.
- [122] M. Zhang, M. Wang, Z. Yang, J. Li, H. Qiu, *J. Alloys Compd.* **2018**, *748*, 537.
- [123] J. Shi, W. Ge, Y. Tian, M. Xu, W. Gao, Y. Wu, *Small* **2021**, *17*, 2006568.



Riccardo Montecucco received his M.Sc. in chemical sciences from the University of Pavia in 2019, with a dissertation on operando X-ray absorption spectroscopy applied to cobalt-based molecular photocathodes for artificial photosynthesis. In 2020, he started the Ph.D. scholarship funded by Eni S.p.A. in chemistry, at the University of Pavia, under the supervision of Giulia Grancini. Currently, he is working on all-inorganic cesium-based perovskites for efficient, stable, and scalable solar cells.



Eleonora Quadrivi received her M.Sc. in physics from the University of Milano-Bicocca in 2018. In 2019, she obtained her second level specializing master's degree in energy innovation from Politecnico di Milano and Eni S.p.A. Now, she is a researcher in solar energy at Eni S.p.A and her activity mainly focuses on the development of efficient and stable perovskite solar cells with particular attention for scalable deposition techniques.



Riccardo Po studied industrial chemistry at the University of Pisa, where he received his M.Sc. in 1988. Subsequently, he joined the materials department of Enichem Research Center in Novara, where he worked on polymer synthesis and modification. In 1999, he became the manager of the polymer chemistry and physics department. In 2007, the research center was incorporated by Eni S.p.A, and he was appointed the manager of the solar energy department and put in charge of the research activities on polymer solar cells. He is currently a senior scientist and is involved in several company's projects involving the development of novel materials for energy applications.



Giulia Grancini is an associate professor in chemistry at the University of Pavia, leading the PVsquared2 team and the ERC Project "HYNANO" developing advanced hybrid perovskites solar cells. She obtained her Ph.D. in physics from Politecnico di Milano in 2012 and worked as a postdoc researcher at IIT in Milano. From 2015 to 2019, she joined the EPFL awarded by SNSF with the Ambizione Energy Grant. She is currently the USERN ambassador for Italy and a board member of the Young Academy of Europe. In 2019 and in 2020 she has been selected among the highly cited scientists from Web of Science. More information can be found at <https://pvsquared2.unipv.it>.